공학박사 학위논문

Studies on performance and degradation of Pd-Pt core-shell electrocatalyst in polymer electrolyte membrane fuel cells

고분자 전해질 연료전지를 위한 팔라듐-백금 코어-쉘 전기화학촉매의 성능 및 열화 현상에 대한 연구

2012 년 8 월

서울대학교 대학원

화학생물공학부

조 윤 환

Abstract

Studies on performance and degradation of Pd-Pt core-shell electrocatalyst in polymer electrolyte membrane fuel cells

Yoon-Hwan Cho

School of Chemical and Biological Engineering

The graduate school

Seoul National University

Polymer electrolyte membrane fuel cells (PEMFCs) are attractive power generator for automotive and stationary applications. However, the high manufacturing costs and insufficient durability of PEMFC are the major barriers to commercialization. Therefore, the development of new catalysts in PEMFC is necessary to enhance the activity and stability as well as reduce the loading amount of Pt. The core-shell structure catalysts have been studied for fuel cell applications because they can reduce the cost of the catalyst and increase the catalytic activity. However, applications in the

practical system such as single cell and degradation test of core-shell catalysts have been rarely reported.

This thesis describes the performance and degradation characteristics of core-shell catalyst in practical system. The membrane electrode assemblies (MEAs) of catalyst coated membrane type were fabricated with Pd-Pt core-shell catalyst and commercial Pt/C as cathode, which were applied to single cell. In order to evaluate the performance and degradation characteristics of core-shell catalyst in single cell, the electrochemical and structure analysis of MEA with core-shell catalysts were conducted before and after accelerated degradation test (ADT). To understand the degradation tendency of core-shell catalyst and pure Pt, ADT was performed using load cycling. Before and after ADT, the structure analyses were conducted by high resolution-transmission microscopy (HR-TEM), X-ray diffraction (XRD), X-ray photoelectron spectroscopy (XPS), and field emission-scanning electron microscopy (FE-SEM) with energy dispersive X-ray (EDX). And the electrochemical characteristics were evaluated by current-voltage characteristics and cyclic voltammetry (CV).

The initial single cell performances of Pd-Pt[0.5] and Pd-Pt[0.7] were 440 mA cm^{-2} and 400 mA cm^{-2} at 0.7 V, which were comparable to the performance of Pt MEA (455 mA cm^{-2}) due to the loading amount of Pt. In the results of the ADT, the decrement rate of performance with Pt MEA was 39% and those with Pd-Pt[0.5] and Pd-Pt[0.7] were 45% and 40%,

respectively. In initial 10 h under ADT, the performance of Pt MEA was decreased 25%, while those of Pd-Pt[0.5] and Pd-Pt[0.7] were 12% and 1% , respectively. After the initial rapid decrease, the performance of Pt MEA was slowly and gradually declined. On the other hand, the performances of Pd-Pt[0.5] and Pd-Pt[0.7] were steadily decreased during the entire operating time of ADT. The electrochemical surface area (ESA) of Pt MEA reduced significantly whereas the decrement rate of ESA of Pd-Pt MEAs was negligible. This loss of ESA in Pt/C was related to the decrease of single cell performance. After the ADT, the particle sizes of Pd-Pt core-shell and Pt nanoparticles were increased. The increasing extents of Pd-Pt core-shell nanoparticles were smaller than those of Pt nanoparticles. In XPS and FE-SEM with EDX, the composition ratios of Pd and Pt were changed after ADT and the Pd band was investigated in the membrane. These compositional characterizations suggested that Pd in Pd-Pt core-shell catalysts was dissolved during ADT. The dissolution of Pd would correspond to the decrease of performance in Pd-Pt core-shell catalyst. In the cases of Pd-Pt[0.5]/C and Pd-Pt[0.7]/C, the performance of Pd-Pt[0.7] was more stable than Pd-Pt[0.5], which might be affected by the amount of Pt deposition. The stability of Pd-Pt core-shell catalysts was good accordance with the results of XRD and the change in atomic ratio before and after ADT.

Keywords: Polymer electrolyte membrane fuel cell (PEMFC),

performance degradation, accelerated degradation test (ADT), membrane electrode assembly (MEA), core-shell catalyst

Student Number: 2006-30867

Contents

List of Tables

List of Figures

Chapter 1. Introduction

1.1 Basic of Fuel Cells

Fuel cell is an electrochemical device that converts the chemical energy of fuel directly into the electrical energy without moving parts. The lack of moving parts allows a simple design, silent operation and high conversion efficiency. Also, fuel cell dose not emit undesirable products such as NO_x and SO_x when pure hydrogen and oxygen are supplied as fuel and oxidant. Unlike other electrochemical devices, a fuel cell can continuously generate electricity as long as reactants are supplied. According to these advantages, fuel cells are attractive as energy sources for various applications, such as transportation, power plant and potable power. Fig. 1.1 shows the various application fields for fuel cell.

There are five major types of fuel cells, distinguished from one another by the electrolyte employed: polymer electrolyte membrane fuel cell (PEMFC), phosphoric acid fuel cell (PAFC), alkaline fuel cell (AFC), molten carbonate fuel cell (MCFC), and solid oxide fuel cell (SOFC). However, all the five fuel cell types are based on the similar electrochemical mechanism and structure although they operate at different temperature and involve different materials. Table 1.1 shows the characteristics of the major fuel cell types.[1-5]

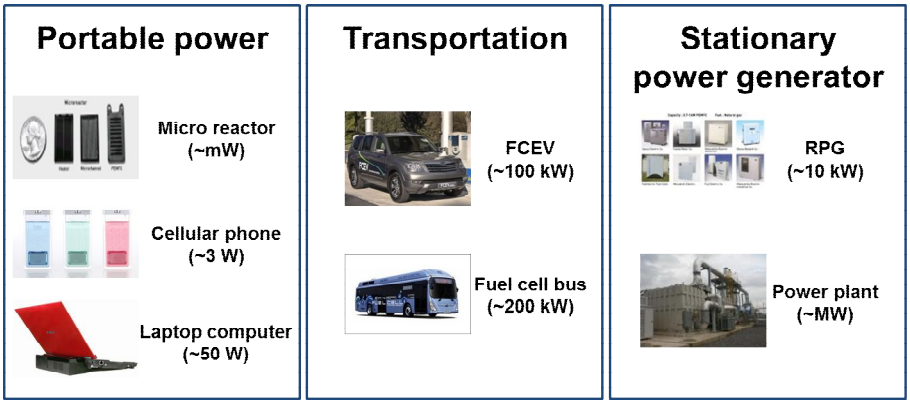

Fig. 1.1. Application fields for fuel cell.

Table 1.1. Characteristics of the major fuel cell types.

	PEMFC	PAFC	AFC	MCFC	SOFC
Electrolyte	Solid polymer membrane	Liquid phosphoric acid soaked in matrix	Liquid potassium hydroxide soaked in matrix	Molten carbonate	Ceramic
Charge carrier	H^+	H^+	OH^-	CO_3^{2-}	O^{2-}
Operating temperature	80 °C	150-200 °C	60-220 °C	650 °C	600-1000 °C
Catalyst	Platinum	Platinum	Platinum	Nickel	Perovskites (ceramic)
Cell components	Carbon based	Carbon based	Carbon based	Stainless based	Ceramic based
Fuel	H_2, methanol	H_2	H_2	H_2, CH_4	H_2, CH_4 , CO

1.2 Polymer Electrolyte Membrane Fuel Cells

1.2.1 Cell Components

A typical PEMFC unit cell consists of the following components: polymer electrolyte membrane (PEM), electrocatalyst in catalyst layer, gas diffusion layer (GDL), flow channels (bipolar plate) and current collector. Fig. 1.2 shows the schematic of PEMFC.

The PEM is located between anode and cathode catalyst layer. This solid polymer electrolyte transports the protons from anode to cathode and supports the anode and cathode catalyst layers. It also separates the oxidizing and reducing environments on the cathode and anode reaction zone. Therefore, the PEM is required high proton conductivity, low gas permeability, mechanical, thermal and chemical stability, and so on.[6-8] The most commonly used PEMs are perfluorosulfonic acid membrane such as Nafion (Dupont), Gore-Select (Gore), and Aciplex and Flemion (Asahi).

The catalyst layers are middle of the membrane and the backing layers. Carbon supported Pt and binary or ternary Pt metal alloys are widely used as electrocatalysts in PEMFCs. The carbon support plays an important role in electrocatalyst. It provides the catalyst dispersion and has effect on increasing of catalyst utilization. From the result of using carbon support, the

loading amounts of Pt are greatly reduced in PEMFC. The carbon materials have effect on the properties of supported metal catalysts, such as metal particle size, morphology, size distribution, dispersion and stability. Carbon blacks are generally used as supports for catalysts such as Vulcan XC72 (Cabot), Black Pearls 2000 (Cabot), and Ketjen EC300J (Ketjen Black).[9]

The GDL is placed in contact with the catalyst layer. It provides the mechanical support for catalyst layer, an electrical pathway for electrons, and a flow channel for product water and reactant gas. Therefore, the GDL is required mechanical stability, flexibility, and high conductivity. Typically, water proofed carbon paper or carbon cloth is used as the GDL. The GDL is prepared with hydrophobic material such as polytetrafluoroethylene (PTFE) in porous structure to improve the gas diffusion and water management.

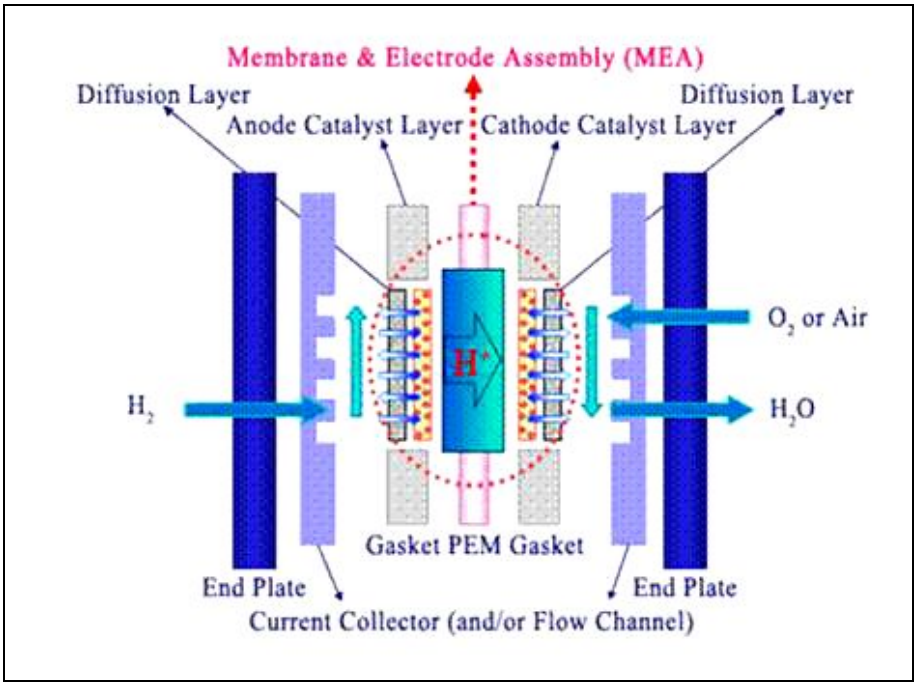

Fig. 1.2. Schematic of PEMFC.

1.2.2 Electrode Reactions

The anode reaction in a PEMFC is hydrogen oxidation reaction (HOR) at the surface of the anode electrocatalyst.[10] The mechanism of anode reaction is described by following three elementary steps: Tafel step (recombination reaction), Volmer step (charge transfer reaction), and Heyrovsky step (ion plus atom reaction). The overall reaction can be expressed as:

$$H_2 + 2H_2O \leftrightarrow 2H_3O^+ + 2e^-$$

The overall process can be consisted of five steps as following:

(1) The transport of the H_2 molecules to the Pt electrode through gas diffusion

(2) The adsorption of hydrogen molecules to the anode electrocatalyst through gas diffusion

(3) The dissociative adsorption of hydrogen on the surface of electrocatalyst through the Tafel reaction

$$Pt - Pt + H_2 \leftrightarrow Pt - H + Pt - H$$

(4) The ionization of H atom giving one electron to the electrode and a hydronium ion to the solution, leaving an empty Pt site through the Volmer

reaction

$$Pt - H + H_2O \leftrightarrow Pt + H_3O^+ + e^-$$

or direct reaction of hydrogen molecules through Heyrovsky reaction

$$Pt + H_2 + H_2O \leftrightarrow Pt - H + H_3O^+ + e^-$$

(5) The transport of the hydronium ions from the phase boundary to the electrolyte solution phase

The cathode reaction in a PEMFC is oxygen reduction reaction (ORR) at the surface of cathode electrocatalyst. The overall four electron of oxygen in acid electrolyte expressed as:

$$O_2 + 4H^+ + 4e^- \rightarrow 2H_2O,\ E^0(O_2/H_2O) = 1.23\ V$$

However, the ORR is a multi-step reaction that can be consisted of several elementary steps.[11] In acidic media, ORR can be described as follows:

The direct four electron pathway

$$O_2 + 4H^+ + 4e^- \rightarrow 2H_2O,\ E^0(O_2/H_2O) = 1.23\ V$$

The peroxide pathway

$$O_2 + 2H^+ + 2e^- \rightarrow H_2O_2,\ E^0(O_2/H_2O_2) = 0.67\ V$$

followed by further reduction or a chemical decomposition via

$$H_2O_2 + 2H^+ + 2e^- \rightarrow 2H_2O,\ E^0(H_2O_2/H_2O) = 1.77\ V$$

$$2H_2O_2 \rightarrow 2H_2O + O_2$$

Many studies have been developed to describe the ORR with several different models. Bagotskii et al. prospered a general scheme for the reactions of O_2 and H_2O_2 as shown in Fig. 1.3.[12, 13]

In this scheme, O_2, $(O_2)_*$, and $(O_2)_a$ represent molecular O_2 in the bulk solution, in the solution adjacent to the electrode surface, and in the adsorbate state, respectively. The oxygen can be reduced directly to water without formation of intermediate or with the formation of intermediate.

The pathway of ORR depends on the pH of the electrolyte and the catalyst. Usually, both the direct and peroxide pathway are found on platinum, platinum alloys, palladium, and silver.

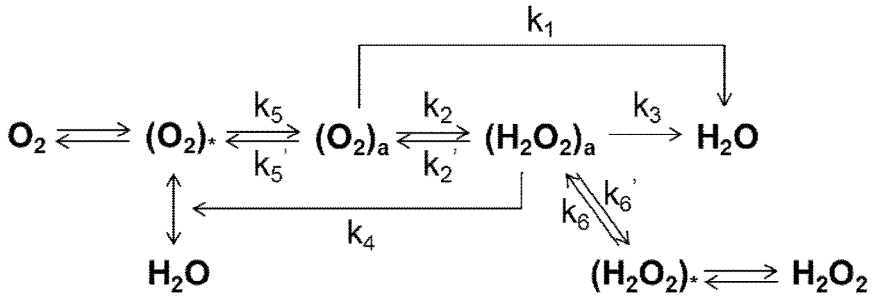

Fig. 1.3. Scheme of oxygen reduction reaction.

1.2.3 Challenges of PEMFC

Polymer electrolyte membrane fuel cells (PEMFCs) are attractive power generators for vehicles, electronic devices, and stationary power generators on account of their low operating temperature and high efficiency of energy conversion

On the other hand, the commercialization of PEMFCs requires an increase in the lifespan of the membrane electrode assembly (MEA) on the PEMFC as well as a decrease in manufacturing cost. The cost of novel metals, especially platinum is one of the most important barriers to the commercialization of PEMFC.[14-17]

The synthesis of Pt alloy catalysts, development of non Pt catalysts, and the reduced use of Pt catalysts through optimization of the catalyst layer structure to a three-phase boundary are effective ways of reducing the MEA cost.[18-21] The cathode catalysts for the oxygen reduction reaction (ORR) have been studied extensively to minimize the use of Pt in the MEA because the ORR is considered the kinetic limit for PEMFCs. For instance, Pt based metal alloy catalysts with transition metals such as PtCo/C, PtNi/C, PtCr/C, and PtFe/C were employed to improve the ORR activity.[22-24]

In addition, MEA fabrication methods were modified, and additives were used to increase Pt utilization and optimize the structure of the catalyst

layer.[25-33] For example, the use of a pore former in the catalyst layer has been reported to improve the performance and transfer of reactants through the catalyst layer. In the MEA fabrication process, a pore former, such as ammonium carbonate, lithium carbonate, ammonium sulfonate or ammonium oxalate, was added to the catalyst ink and removed by a heating process or specific solvent after fabricating the catalyst layer. The prepared catalyst layer exhibited the enhanced performance and lowered the mass transfer resistance due to the morphological modification.[34-38]

1.3 Pd Electrocatalyst in Fuel Cells

Recently, Pd based alloy catalysts have much attention for fuel cell applications. Pd and Pt have similar properties because they belong to the same group of the periodic table. They have the same fcc crystal structure and similar atomic size. However, the cost of Pd is lower than that of Pt as shown in Fig. 1.4.[39] Pd is also fifty times more abundant in the earth's crust than Pt.[40] Pd based metal alloy catalysts have been reported to significant electrocatalytic activity. For example, Pd based metal alloy catalysts such as PdPt/C, PdCo/C, PdFe/C, PdNi/C, and PdPtNi/C have been studied as the substitutes for Pt.[41-43] In the case of PdCo/C and PdFe/C, the ORR activities of the prepared catalysts were similar to that of Pt/C in PEMFCs. Shao et al. investigated the ORR activity of PdFe/C alloy electrocatalyst. The activity of the Pd_3Fe/C was comparable to that of commercial Pt containing catalyst.[44] The ternary Pd-Co-based catalysts also studied to apply the cathode in PEMFCs. Pd-Co-Au catalyst showed comparable ORR activity to that of a commercial Pt/C.[45] The HOR activity of Pd based alloy catalysts also has been investigated.[46-54] Cho et al. suggested that using carbon supported 60 wt.% $Pd_{95}Pt_5$ electrocatalyst as an anode in PEMFC is a promising alternative material that would not sacrifice the HOR activity[49, 50] Yoo et al. reported that Pd in PtPd alloy modified the electronic structure of Pt, which

affected to improve the HOR activity.[54]

In addition, Pd based metal alloy catalysts have shown inactive for the adsorption and oxidation of methanol.[55-62] For example, PdCo catalysts have been studied as a methanol tolerant cathode catalyst in DMFCs. In the presence of methanol, the PdCo/C catalysts showed higher ORR activity than Pt/C due to the lower activity of Pd for the MOR. Also, PdPt catalysts have been reported to be capable of being used as ORR catalysts in DMFCs due to the high activity for ORR and methanol tolerance properties.

However, the enhancement of durability in Pd is necessary to apply the fuel cell. The studies reported that Pd was dissolved under the fuel cell operating conditions. The dissolved Pd ion affected the membrane conductivity and degradation of performance.[41, 63]

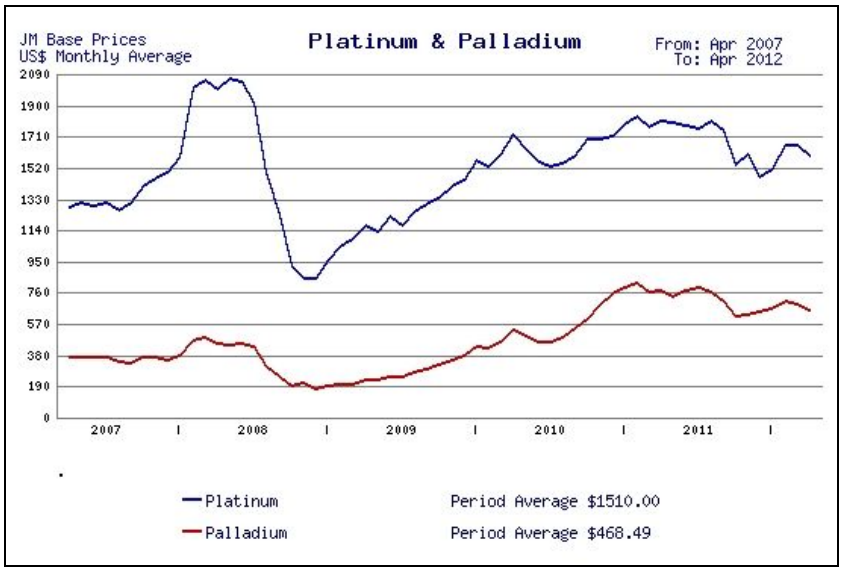

Fig. 1.4. Price chart of platinum and palladium during 2007 to 2012.

1.4 Degradation Mechanisms of MEA Components

The increase of fuel cell lifetime is the important issue to commercialize the fuel cell. The requirement for PEMFC stack lifetime is 5000 h for car, 20,000 h for bus application and 40,000 h for stationary application. According to US Department of Energy (DOE) technical target for fuel cell stack system, the requirement of PEMFC stack lifetime is 5000 h by 2010. Many researches have been studied about degradation of fuel cell to increase the lifetime and understand the degradation mechanism of each component such as membrane, electrode and bipolar plate and so on.[64-77]

The major cause for failure in membrane is chemical degradation.[5, 78] In chemical degradation, hydroxyl (OH) and peroxy (OOH) radicals generated during the reaction attack the polymer end groups that still contain residual terminal H-groups. Curtin et al. showed an example of radical attack on carboxyl end groups:[79]

$$R_f\text{-}CF_2COOH + OH\cdot \rightarrow R_f\text{-}CF_2\cdot + CO_2 + H_2O$$

$$R_f\text{-}CF_2\cdot + OH\cdot \rightarrow R_f\text{-}CF_2OH \rightarrow R_f\text{-}COF + HF$$

$$R_f\text{-}COF + H_2O \rightarrow R_f\text{-}COOH + HF$$

As repeated the radical attack, the polymer may decompose into low

molecular weight compounds. Mechanical degradation of membrane is also caused by non-uniform contact pressure, fatigue from stresses occurring temperature and humidity. The mechanical stresses may lead to the thinning of the membrane and increased hydrogen crossover.[80]

The predominant mechanisms of electrode degradation are the dissolution and particle growth of Pt, oxidation of carbon support and dissolution of metal from Pt metal alloy catalysts. Several studies conducted to understand the dissolution and particle growth of Pt during the PEMFC operation.

One of the proposed degradation mechanisms is Ostwald ripening. Small Pt particles may dissolve in the ion phase and redeposit on the surface of large Pt particles. This process leads particles growth of Pt. The Pt dissolution in acid media strongly increases with potential in the region of 0.85-0.95 V versus RHE. Meyers and Darling showed that Pt dissolution in PEMFCs was negligible at low and high potentials, whereas substantial Pt was dissolved at intermediate potentials.[81] They considered following reactions:

$$Pt \rightarrow Pt^{2+} + 2e^{-} \text{ (platinum dissolution)}$$

$$Pt + H_2O \rightarrow PtO + 2H^{+} + 2e^{-} \text{ (platinum oxide film formation)}$$

$$PtO + 2H^{+} \rightarrow Pt^{2+} + H_2O \text{ (chemical dissolution of platinum oxide)}$$

From the model and experimental data, the solubility of Pt in acid is low at lower potentials. And at higher potentials, the oxide layer insulates the Pt dissolution. However, the uncovered surface is prone to high rates of Pt dissolution at intermediate potentials.

The dissolved Pt may diffuse into the ionomer phase and precipitation within the membrane, which called as Pt band. The formation of Pt band decreases membrane stability and conductivity.[82] The sketch of degradation mechanisms about the Ostwald ripening and precipitation in the ionomer phase are shown in Fig. 1.5.

Another mechanism of particle growth is coalescence, which is proposed in some PEMFC studies. In this mechanism the Brownian motion is the driving force, causing the surface diffusion of particles with random collisions leading to coalescence.[83, 84] In PEMFC operations, the potential and increased humidity enhance the particle growth.

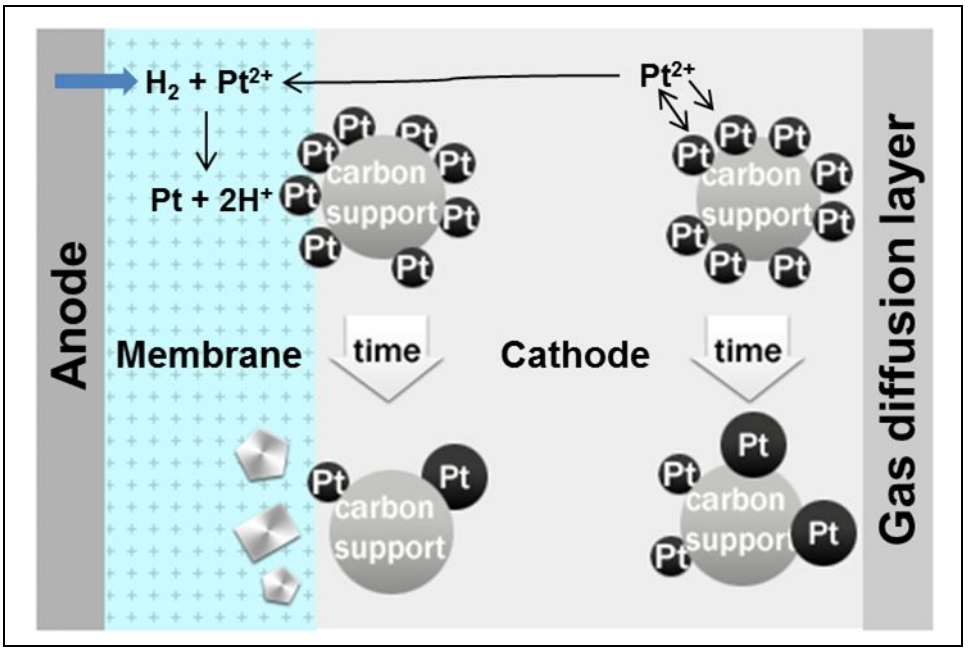

Fig.1.5. The sketch of degradation mechanism about the Ostwald ripening and precipitation in the ionomer phase.

Electrochemical corrosion of the carbon support is important issue for durability of electrocatalyst and catalyst layer in PEMFCs. Thermodynamically, carbon oxidation to CO_2 occurred at quite low potentials:

$$C + 2H_2O \leftrightarrow CO_2 + 4H^+ + 4e^-, E^0=0.207\ V$$

Despite the thermodynamic instability, carbon can still be used in fuel cell due to the slow kinetics of carbon corrosion.[85] However, under the start-up and shutdown conditions, the cathode potential can reach as high as 1.5 V, leading to extensive carbon support oxidation. The PEMFC operating conditions also have a negative effect on durability of carbon. The operating conditions include high water content, low pH, high temperature, high oxidative potential, and high oxygen concentration.

The corrosion of carbon leads to a reduction of the carbon content in the catalyst layer with time. And metal nanoparticles in electrode may be lost or aggregated to larger particles. Oxidation of carbon can also lead to changes in hydrophobicity of catalyst layer that have effect on the mass transport.

Carbon supported Pt metal alloy catalysts are developed to improve the kinetics of ORR and lower the Pt loading. However, Pt metal alloy catalysts

are reported the dissolution of non-precious metal in the acid media, which leads to decrease of the performance. Popov and coworkers reported the durability of Pt_3Ni/C under degradation test.[86, 87] After the test, the decrease in catalytic activity of Pt_3Ni/C was correlated to Ni dissolution in the electrolyte. Gasteiger et al. reported the base metal loss mechanism of Pt metal alloy catalysts. They suggested three possible causes for the leaching of base metal from Pt metal alloy catalysts in PEMFCs as following:[18]

1. Excess base metal deposited onto the carbon support during preparation
2. Incomplete alloying of the base element to Pt
3. Thermodynamically unstable base metal under PEMFC operating conditions

The durability studies in PEMFCs can be challenging because of the prolonged test period and complexity of failure analysis. Therefore, accelerated degradation tests (ADTs) are developed to understand the degradation mechanism and provide a valuable tool for significantly reducing the extent of experiments in the lifetime evaluation and degradation mode analysis.[88, 89] The factors of ADTs may include the operation temperature, operation voltage or current density. Gasteiger et al. proposed the catalyst potential cycling test and support corrosion test at 1.2 V to measure the

degradation of fuel cell catalyst. They suggested that the potential cycling test was more related to drive cycle of PEMFC on vehicles than the constant current or constant potential test.[90] In catalyst potential cycling test, the cycling range of potential affected the degradation ratios of MEA. The performance degradation under potential cycling test is more severe than that under the constant current or constant potential test.

1.5 Objectives of This Thesis

As discussed in previous sections, for the commercialization of PEMFC, it is necessary to reduce the manufacturing cost of the fuel cell and maintain stable operation.

To alleviate these problems, synthesized Pd-Pt core-shell catalysts were applied to single cell and degradation test in this study. Recently, the studies of core-shell structure catalysts have much attention for fuel cell applications due to the many advantages.[91-94] The core-shell structure can reduce the cost of the catalyst using low cost metal for core and novel metal for shell. Also, this structure has effect on the catalytic activity and dispersion of the shell particle. The synthesized Pd-Pt core-shell catalysts with different loading of Pt shell were characterized using the X-ray diffraction, energy dispersive spectroscopy, X-ray photoelectron spectroscopy, high resolution-transmission electron microscopy, cyclic voltammetry, and single cell tests. The performance degradation of Pd-Pt core-shell catalyst was investigated with load cycling test in single cell. The degradation tests in half cells are important to estimate the electrochemical characteristics of catalysts. However, the test in single cell is more practical than that in half cell. Because the operating conditions such as temperature, pressure and fuel flows are crucial to determine the real performance of a system. To understand the durability

and degradation tendency of the core-shell catalysts, the electrochemical and structure analysis of MEA with core-shell catalysts were conducted before and after ADT.

Chapter 2. Experimental

2.1 Fabrication of Membrane Electrode Assembly

2.1.1 Synthesis and Characterization of Pd-Pt Core-Shell Catalysts

The carbon supported Pd-Pt core-shell nanoparticles for cathode catalysts were prepared as follows: First, Pd/C (28.4 wt.%) was prepared through the borohydride reduction in anhydrous ethanol. And then, Pt deposited on the carbon supported Pd nanoparticles using hydroquinone. For the formation of the Pt shell, Pd/C was dispersed in 20 mL of anhydrous ethanol and sonicated for 10 min. After additional stirring for 10 min, platinum (IV) chloride ($PtCl_4$) and hydroquinone ($C_6H_6O_2$), which were dissolved in 60 and 40 mL of anhydrous ethanol, respectively, were added to the solution containing the core materials. The mixture solution was stirred for 1 h. After a final sonication for only 3 min to avoid the reduction of Pt ions, the solution was loaded into a four-neck flask. The solution was then deaerated under Ar stream and heated to 70 °C at the rate of 1.25 °C min^{-1}. Once the temperature of the system reached 70 °C, a heating controller maintained the solution at the constant temperature. The heater was turned off after 2 h of heating. The solution was then cooled, filtered, washed with ethanol (95 %)

at room temperature, and dried at 40 °C in a vacuum oven. Carbon supported Pd-Pt core-shell nanoparticles with Pd to Pt atomic ratios of 1:0.5 (Pd-Pt[0.5])and 1:0.7 (Pd-Pt[0.7]) were synthesized and 40 wt. % carbon supported Pt (40 wt. % Pt/C) catalyst was purchased from Johnson Matthey.

The synthesized Pd-Pt/C core-shell catalysts and purchased Pt/C catalyst were characterized by the X-ray diffraction (XRD) and high resolution transmission electron spectroscopy (HR-TEM). XRD patterns were taken by Powder X-Ray Diffractometer (Rigaku D/MAX 2500) using the CuKα source at 40 kV and 100 mA. The catalysts were scanned from 20 to 80° with a 2° min^{-1}. The particle size and dispersion of the synthesized catalysts were observed by HR-TEM (JEOL 2010). The HR-TEM analysis was performed with working at 200 kV accelerating potential.

2.1.2 Fabrication of Catalysts Ink

The catalyst inks of cathode were fabricated ultrasonically using the synthesized Pd-Pt/C core-shell catalysts and commercial Pt/C catalyst, 5 wt.% Nafion solution (Aldrich Chem. Co), D.I. water and isopropyl alcohol (IPA, Aldrich Chem. Co) as the solvent. The carbon-supported Pt catalyst powder (40 wt.% Pt/C, Johnson Matthey) was used as the catalysts for anode. Anode catalyst inks were prepared by the above method.

2.1.3 Fabrication of Membrane Electrode Assembly

The Nafion 212 membrane was pretreated with the hydro-peroxide solution (3 wt.%) for 1 hr and sulfuric acid solution (0.5 M) for 1 hr at 100 °C. The pretreated membrane was dried and placed in the appropriate frame. For the preparation of MEA, the catalyst inks were sprayed directly onto both sides of the pretreated Nafion 212 membrane to form the catalyst-coated membrane (CCM). The metal catalyst was loaded with 0.2 mg cm^{-2} and 0.3 mg cm^{-2} on anode and cathode electrodes, respectively. The active surface area on the MEA was 5 cm^2. The MEAs with cathode catalyst used in Pt/C, Pd-Pt[0.5]/C and Pd-Pt[0.7]/C were named as Pt MEA, Pd-Pt[0.5], and Pd-Pt[0.7], respectively. The fabrication process of MEA is showed in Fig. 2.1.

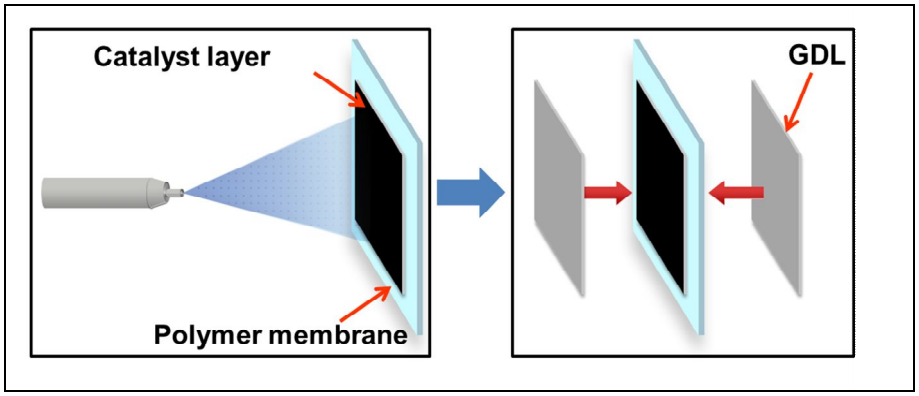

Fig. 2.1. Fabrication process of MEA.

2.2 Electrochemical Analysis

2.2.1 Current-Voltage Characterization

The single cell performance of each MEA with a geometric area of 5 cm^2 was measured. The MEA was placed between two gas diffusion layers (GDLs, E-TEK) and inserted into the graphite plates that contained serpentine flow channels. The single cell was assembled by a torque wrench due to the same pressure at the moment of setting the cell. Fig. 2.2 is a photograph of single cell in this study. The single cell was then connected to a fuel cell test station (FCTS, WonATech Co., Ltd.). For performance measurements, humidified H_2 and air were fed to the anode and cathode with a stoichiometric ratio of 1.5 / 2 at a temperature of 75 / 70 °C. The cell temperature was set at 70 °C and backpressure on the single cell was at ambient conditions. The cell voltage of each MEA was obtained with the increasing current density using fuel cell test station to measure the current-voltage curves. Fig. 2.3 shows a photograph of fuel cell test station.

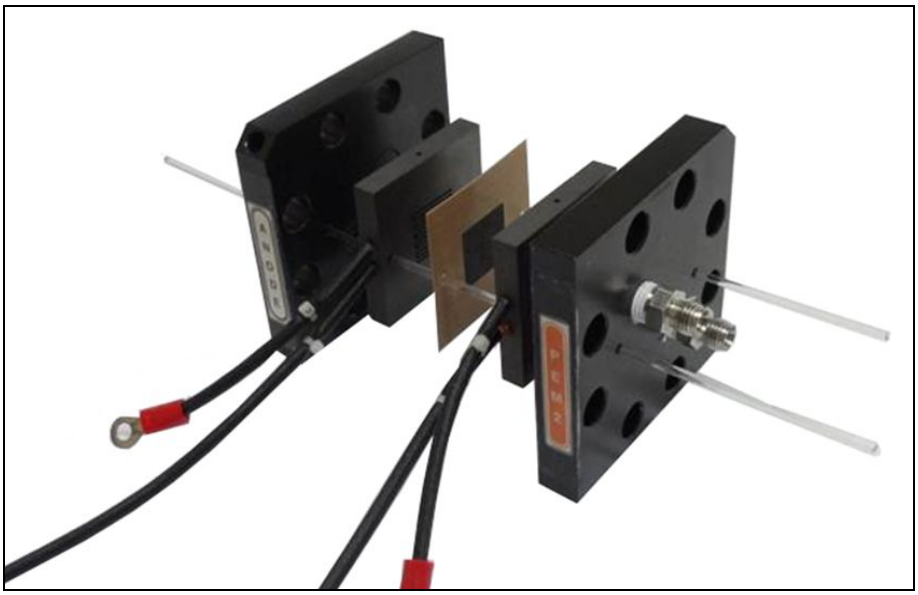

Fig. 2.2. Photograph of single cell with MEA.

Fig. 2.3. Photograph of fuel cell test station.

2.2.2 Accelerated Degradation Test of Single Cell

To investigate the degradation characteristics of the MEA performance with Pt/C, Pd-Pt[0.5]/C and Pd-Pt[0.7]/C as cathode catalyst, ADT was performed with prepared MEA for 50 h. The ADT was carried out using the repetition of load cycling which consisted of increasing the cell current with 50 mA s^{-1} from OCV to 0.35 V, and shut-off the load and then remaining OCV for 30 sec. The operating conditions of ADT were the same as the current-voltage characterization.

Cyclic voltammetry (CV) was carried out to estimate the electrochemical surface area (ESA) of each MEA before and after ADT. CV was performed in the scan range from 0.00 to 0.95 V at a scan rate of 100 mV s^{-1}. Humidified H_2 was fed into the anode as the reference electrode, and humidified N_2 was fed into the cathode as working electrode, respectively.

2.3 Structure Analysis

2.3.1 High Resolution-Transmission Electron Microscopy

High resolution-transmission electron microscopy (HR-TEM) was conducted to observe the changes in the morphology, particle size, and size distribution of Pt/C, Pd-Pt[0.5]/C, and Pd-Pt[0.7]/C nanoparticles before and after ADT. The samples were prepared by scraping the catalyst layer to peel off the catalysts from MEA, and then catalysts were suspended in ethanol. The samples were dropped on a carbon film supported on copper grid and evaporated the solvent. HR-TEM images were obtained using a JEOL 2010 at a 200 kV accelerating potential.

2.3.2 X-ray Diffraction Analysis

X-ray diffraction (XRD) analysis was carried out to investigate the change in the crystallite size of Pt/C, Pd-Pt[0.5]/C, and Pd-Pt[0.7]/C before and after ADT. XRD measurement was carried out with a Rigaku D/MAX 2500 using a CuKα source (λ=1.541 Å) at 40 kV and 100 mA. The samples were scanned from 20 to 80° with a 2° min^{-1}.

2.3.3 X-ray Photoelectron Spectroscopy

The valence state and composition of Pd-Pt[0.5]/C and Pd-Pt[0.7]/C after

ADT were determined using X-ray photoelectron spectroscopy (XPS) with an ultrahigh vacuum (UHV) multipurpose surface analysis system (SIGMA PROBE, Thermo, UK) operating at base pressures < 10^{-10} mbar. The photoelectron spectra was excited by an Al Kα (1486.6 eV) anode operating at a constant power of 100 W (15 kV and 10 mA). During the spectra acquisition, the constant analyzer energy (CAE) mode was employed at the pass energy of 40 eV and a step of 0.1 eV. The electron binding energy scale was calibrated from the hydrocarbon contamination using the C 1s peak at 284.6 eV. The core peaks were analyzed using a non-linear Shirley-type background, and the peak position and area were obtained by a weighed least-square fitting of model curves (70 % Gaussian, 30 % Lorentzian) to the experimental data.

2.3.4 Field Emission-Scanning Electron Microscopy with Energy Dispersive X-ray Analysis

The structures of cross-section of Pt MEA, Pd-Pt[0.5], and Pd-Pt[0.7] before and after ADT were examined using field emission-scanning electron microscopy (FE-SEM, JSM 6700F, JEOL Ltd.) to prove the morphological changes of the electrodes and the connection between catalyst layer and membrane.

The chemical composition and the distribution of different elements over the MEA before and after ADT were evaluated using energy dispersive X-ray (EDX; 7421, OXFORD) associated to a FE-SEM.

Chapter 3. Results and Discussion

3.1 Characterization of Catalysts

The synthesized Pd-Pt[0.5]/C, Pd-Pt[0.7]/C and commercial Pt/C catalysts were characterized by HR-TEM to investigate the morphology and size distribution of nanoparticles. Fig. 3.1 and 3.2 show HR-TEM images of synthesized Pd-Pt[0.5]/C and Pd-Pt[0.7]/C catalysts. The metal particles were highly dispersed on the carbon supports (Vulcan XC72). Pd-Pt[0.7]/C catalyst shows more agglomeration of nanoparticles compared to Pd-Pt[0.5]/C catalyst. Fig. 3.3 shows HR-TEM images of commercial 40 wt.% Pt/C catalyst. The spherical shaped platinum particles are well-dispersed on the carbon support. The mean particle size of catalysts was measured from 100 ea. metal particles. Fig. 3.4 shows the particle size distribution histograms based on about 100 nanoparticles. The mean particle sizes of the Pd-Pt[0.5]/C, Pd-Pt[0.7]/C and commercial Pt/C catalysts obtained by HR-TEM are approximately 4.04, 4.37 and 3.83 nm, respectively. As expected, the mean particle size of Pd-Pt[0.7] is larger than that of Pd-Pt[0.5] due to the increase of Pt deposition.

The XRD patterns of the Pd-Pt[0.5]/C, Pd-Pt[0.7]/C and commercial Pt/C catalysts are shown in Fig. 3.5. In all cases, the XRD profiles of the catalysts

showed the main peaks of face-centered cubic (FCC) structure, which had intrinsic peaks for (111), (200) and (220). The (220) peak was used to calculate the mean crystallite size of catalysts with the Scherrer equation because the (111) and (200) peaks with broad C peaks overlap each other.[95] The diffraction peaks of Pd-Pt[0.5]/C and Pd-Pt[0.7]/C were shifted to slightly higher angle compared to those of Pt/C. However, the angle shifts of Pd-Pt[0.5]/C and Pd-Pt[0.7]/C are negligible because Pd and Pt have the same crystal structure and similar peak positions. The mean crystallite sizes of Pd-Pt[0.5]/C, Pd-Pt[0.7]/C and commercial Pt/C obtained from XRD are approximately 3.98, 4.30 and 3.76 nm, respectively. The mean crystallite sizes and (220) peak positions of samples obtained from the XRD are given in Table 3.1.

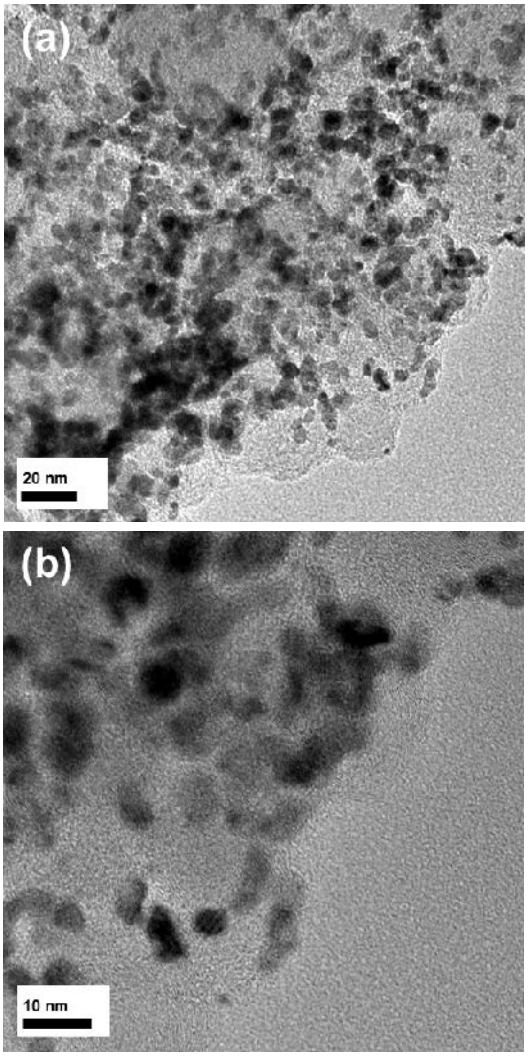

Fig. 3.1. HR-TEM images magnified (a) 120,000 times and (b) 300,000 times of Pd-Pt[0.5]/C catalysts.

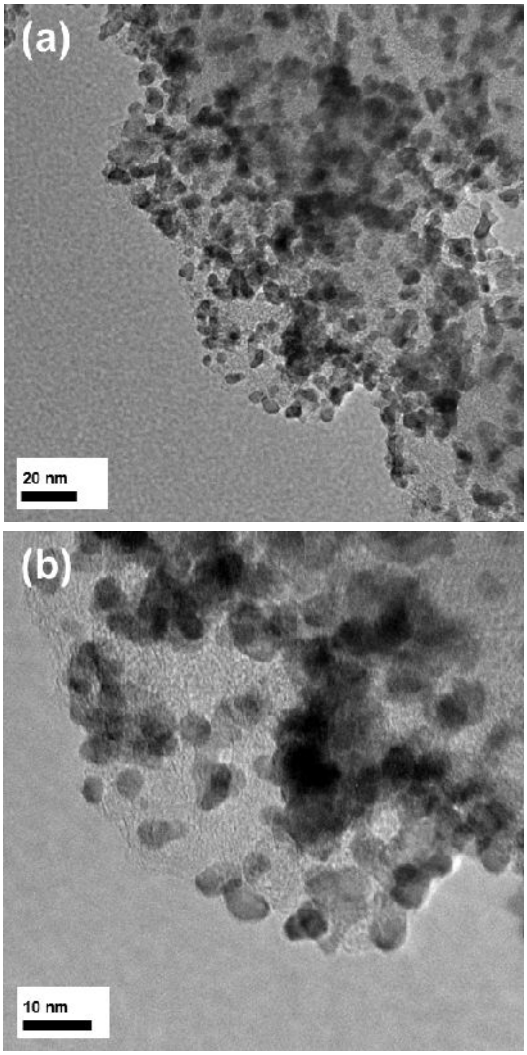

Fig. 3.2. HR-TEM images magnified (a) 120,000 times and (b) 300,000 times of Pd-Pt[0.7]/C catalysts.

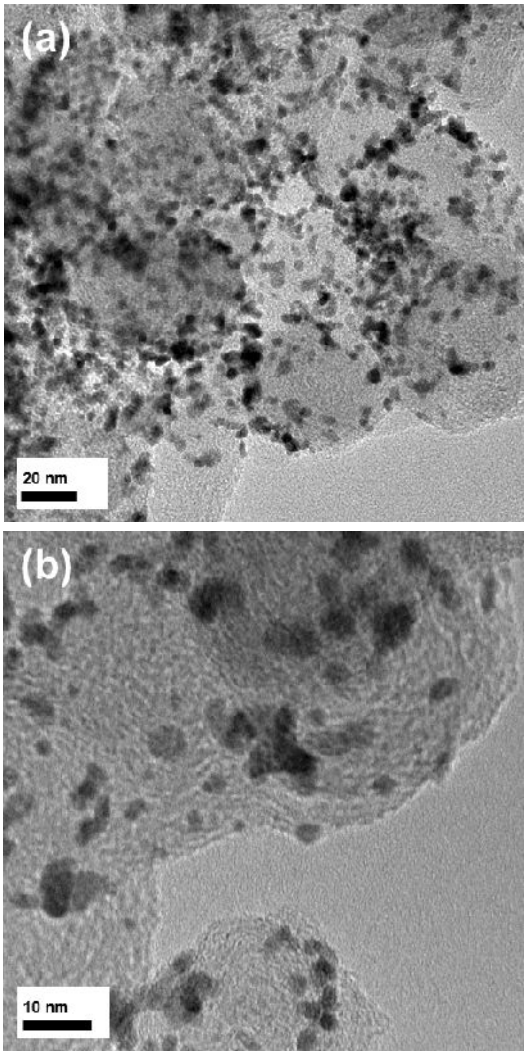

Fig. 3.3. HR-TEM images magnified (a) 120,000 times and (b) 300,000 times of Pt/C catalysts.

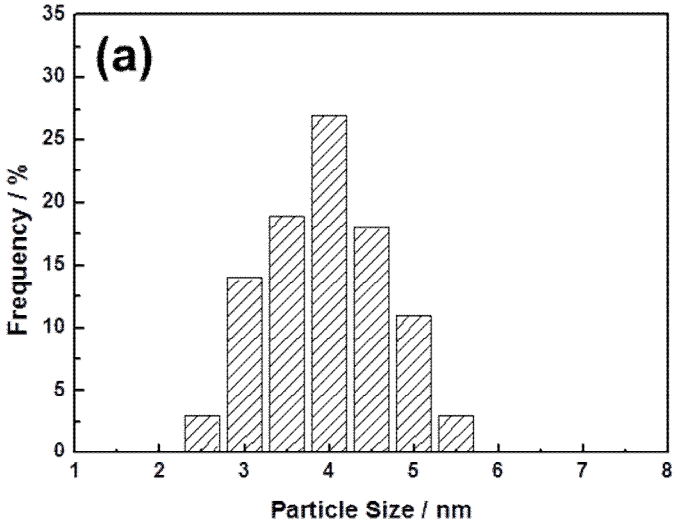
(a)
Frequency / %
Particle Size / nm
0
5
10
15
20
25
30
35
1
2
3
4
5
6
7
8

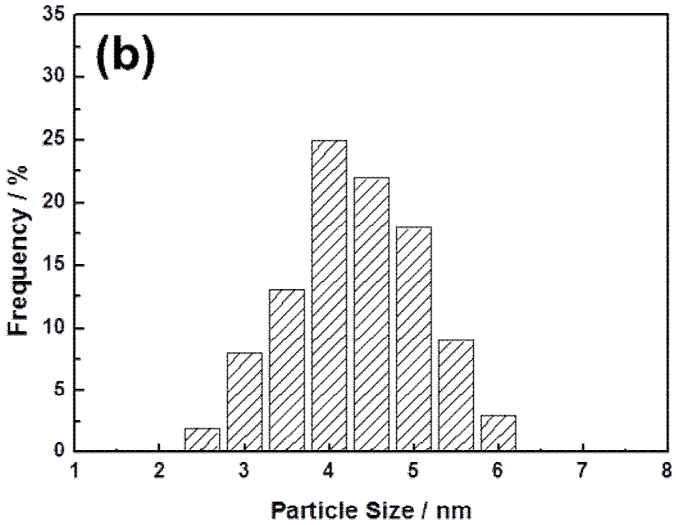
(b)
Frequency / %
Particle Size / nm
0
5
10
15
20
25
30
35
1
2
3
4
5
6
7
8

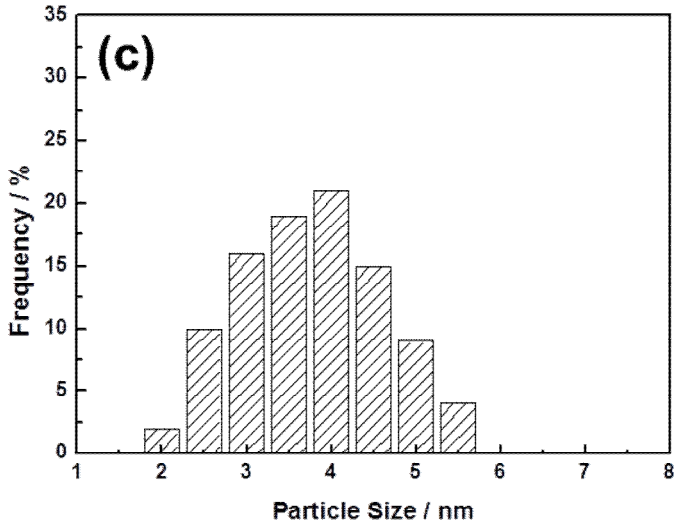

Fig. 3.4. The size distribution histograms of (a) Pd-Pt[0.5]/C, (b) Pd-Pt[0.7]/C, and (c) Pt/C catalysts.

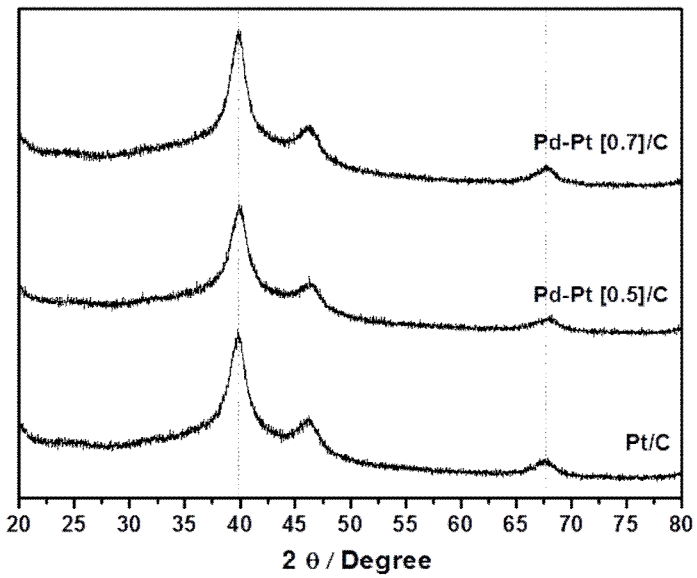

Fig. 3.5. X-ray diffraction patterns of Pd-Pt[0.5]/C, Pd-Pt[0.7]/C, and Pt/C.

Table 3.1. The peak position and mean crystallite size of Pd-Pt[0.5]/C, Pd-Pt[0.7]/C, and Pt/C.

Catalyst	Mean crystallite size / nm	Peak position (220)
Pt/C	**3.76**	**67.46**
PdPt[0.5]/C	**3.98**	**67.66**
PdPt[0.7]/C	**4.30**	**67.60**

3.2 Characteristics of Single Cell Performance under ADT

The polarization curves of initial MEA with Pt/C, Pd-Pt[0.5]/C and Pd-Pt[0.7]/C at specified time intervals (after 10, 20, 30, 40 and 50 h operating) under load cycling are shown in Fig. 3.6, 3.7 and 3.8, respectively. The ADT involved load cycling between 0.35 and OCV with a 30 sec dwell time at 70 °C, and the single cell was continuously connected with fuel cell test station during the test. Cyclic voltammetry was conducted before and after ADT.

Fig. 3.6 presents the polarization curves of Pt MEA at the specified time intervals under ADT. The performance of single cell with Pt MEA decreases with operating time. The cell performance was compared at 0.7 V because the activation kinetics dominated at low current region. The performance of initial MEA was approximately 455 mA cm^{-2} at 0.7 V, while that of MEA after operating for 50 h was 276 mA cm^{-2} at 0.7 V. After the ADT for 50 h, the performance of Pt MEA at 0.7 V decreased 39%. It is worth noting that the decrease of performance is significant during 0-10 h operation and the decrement rate becomes smaller after operating for 10 h. Fig. 3.9 shows the current densities versus time under ADT at 0.7 V. As shown in Fig. 3.9, the decrement rate of Pt during 0-10 h is 25% while that of 10-20, 20-30, 30-40

and 40-50 h is 11, 5, 2, 3%, respectively. This result indicates that the crucial decay of the MEA with Pt/C happens during the period of 0-10 h. The degradation of single cell performance with Pt/C is classified with the recoverable and unrecoverable degradation. The recoverable degradation is a result of transient degradation where the loss of performance may return to pre-degraded levels. For example, the loss of cell performance by water flooding may recovered by eliminating the excess water in GDL. On the other hand, the unrecoverable degradation is an irreversible change to the materials such as decrease of electronic conductivity from carbon corrosion, membrane thinning, and loss of electrochemical surface area from catalyst particle sintering or dissolution.[65-69] In Pt MEA under ADT, the unrecoverable degradation has effect on the initial rapid decrease of performance.

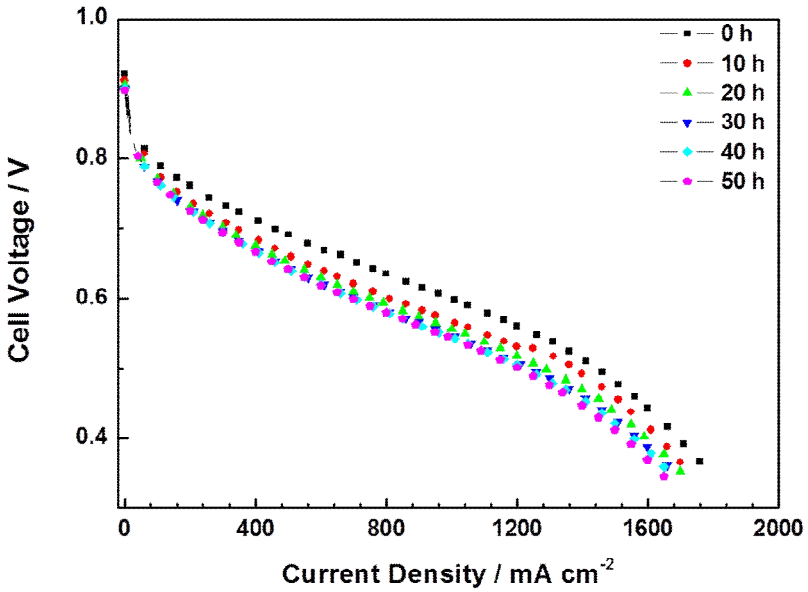

Fig. 3.6. The polarization curves of Pt MEA at specified time intervals under ADT.

Fig. 3.7 and 3.8 show the polarization curves of Pd-Pt[0.5] and Pd-Pt[0.7] with operating time. The initial performances of the cell with Pd-Pt[0.5] and Pd-Pt[0.7] were approximately 440 mA cm^{-2} and 400 mA cm^{-2} at 0.7 V, respectively. The MEA with Pd-Pt core-shell catalyst as cathode catalyst showed slightly inferior single cell performance because the ratios of ionomer and solvent for catalyst layer structures of MEAs were optimized to commercial 40 wt.% Pt/C catalyst. After the ADT for 50 h, the performance of Pd-Pt[0.5] and Pd-Pt[0.7] were approximately 240 mA cm^{-2} and 235 mA cm^{-2} at 0.7 V, respectively. The decrement rate of Pd-Pt[0.5] and Pd-Pt[0.7] were approximately 45% and 40 %. As shown in Fig. 3.9, the MEAs with Pd-Pt core-shell catalysts show the tendency to a steady decline of the performance. The decrement rate of Pd-Pt[0.7] during 0-10 h was only 1% and that of Pd-Pt[0.5] is 12%, which were smaller than that of Pt MEA. On the other hand, the performance of Pd-Pt[0.5] and Pd-Pt[0.7] decreased continuously during 10-50 h whereas the Pt MEA showed the steady performance to the end of the ADT after its initial rapid decay. The decrement rate of Pd-Pt[0.5] was higher than that of Pd-Pt[0.7] in entire region. The declining tendency of Pt MEA and Pd-Pt core-shell MEAs indicates that a different mechanism affects the degradation of Pt/C and Pd-Pt core-shell catalysts. And this result implies that core-shell catalyst used in

MEA may be stable performance in initial operation. The electrochemical and structure analysis will be discussed in the next part.

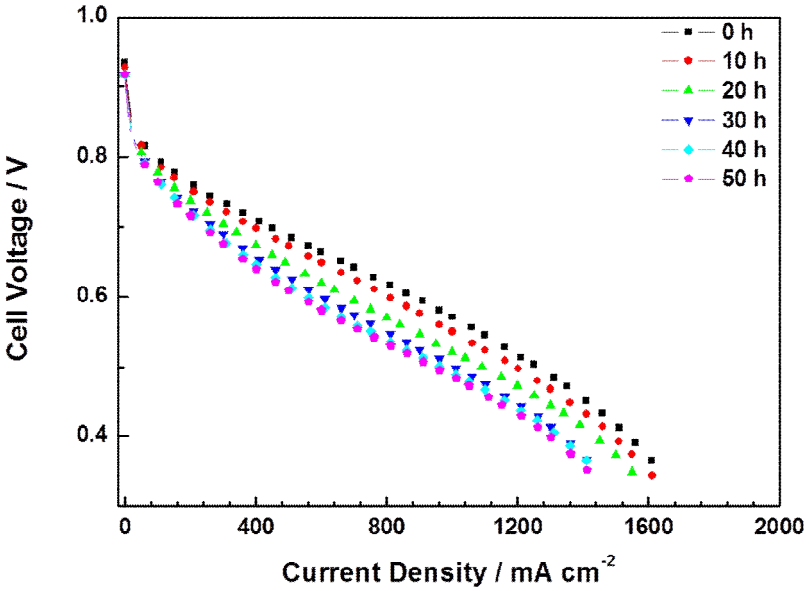

Fig. 3.7. The polarization curves of Pd-Pt[0.5] at specified time intervals under ADT.

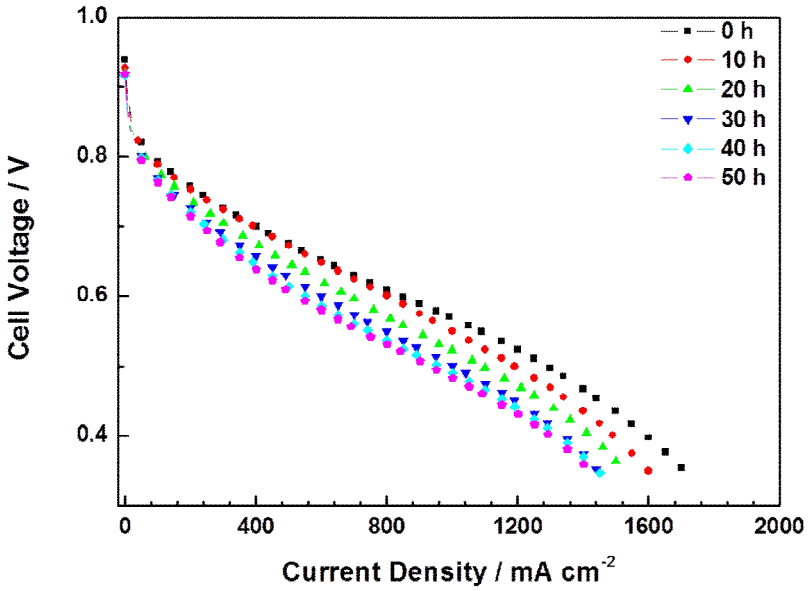

Fig. 3.8. The polarization curves of Pd-Pt[0.7] at specified time intervals under ADT.

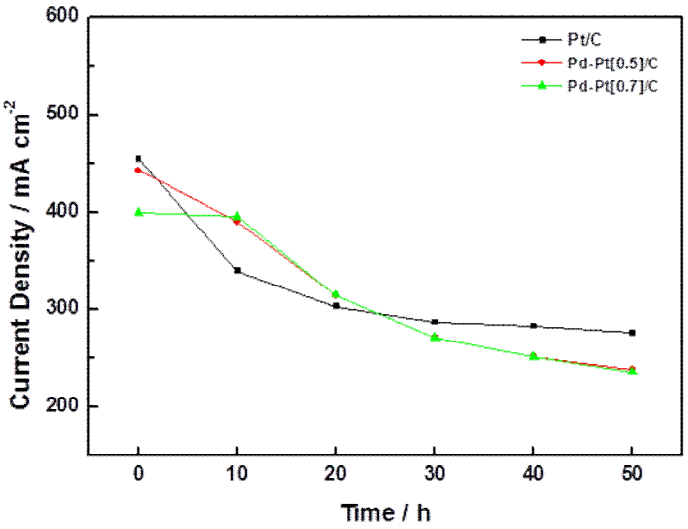

Fig. 3.9. The current densities of single cell with Pt MEA, Pd-Pt[0.5], and Pd-Pt[0.7] as a function of time at 0.7 V.

3.3 Cyclic Voltammetry Results under ADT

To determine the difference in the electrochemical surface area (ESA) of the Pt MEA, Pd-Pt[0.5], and Pd-Pt[0.7] before and after ADT, CV was performed in the scan range from 0.0 V to 0.95 V at a scan range of 100 mV s^{-1}. Fig. 3.10, 3.11, and 3.12 show the CV curves of the Pt MEA, Pd-Pt[0.5], and Pd-Pt[0.7] before and after ADT. The curve shape in the CV of Pd-Pt[0.5] was similar to that of the Pd-Pt[0.7]. The current was normalized to the geometric area of each MEA. As shown in Fig 3.10, well-defined hydrogen adsorption/desorption peaks and peroxidation/reduction peaks were observed. The electrochemical surface area was calculated with the following equation[96]:

$$ESA = Q_H / Q_{ref} L$$

where Q_H is the charge density obtained from the hydrogen adsorption/desorption peaks, Q_{ref} is the charge density associated with the adsorption of protons on Pt (210 μC cm^{-2}) and L is the catalyst loading in the electrode. The ESAs of samples measured from CV are given in Table 3.2. The ESAs of Pt MEA, Pd-Pt[0.5], and Pd-Pt[0.7] before ADT were 33.1 m^2 g^{-1}, 24.3 m^2 g^{-1}, and 29.6 m^2 g^{-1}, respectively. The ESA of the MEA corresponded to Pt content of each catalyst. The decreasing rates of ESA of Pt MEA, Pd-Pt[0.5], and Pd-Pt[0.7] MEA after ADT were 18.7 %, 5.3 %,

and 4.4 %. In the degradation of cell performance and CV results, the decrease of performance in Pt MEA was associated with the loss of ESA. As reported in prior studies, the ESA of Pt MEA reduced significantly.[69, 87] On the other hand, decrement rate of ESA of Pd-Pt core-shell MEAs was negligible. These results suggest that the decrease of the MEA with Pd-Pt core-shell catalyst is not related to the loss of ESA.

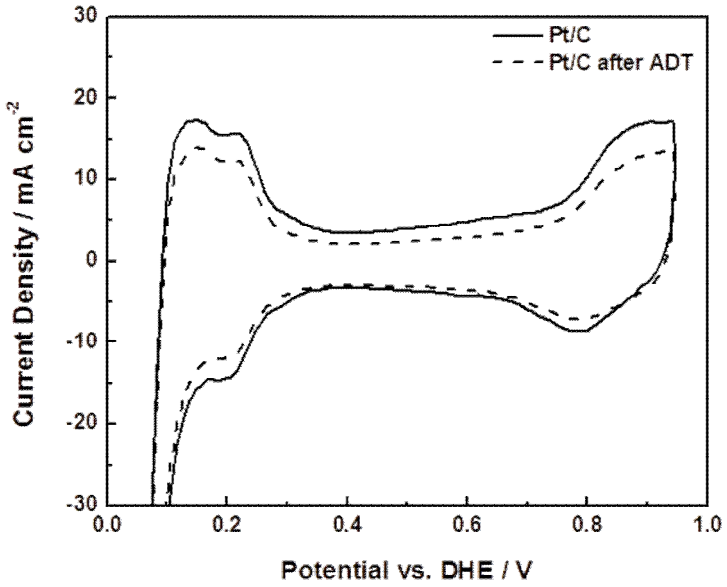

Fig. 3.10. Cyclic voltammograms of Pt MEA before and after ADT.

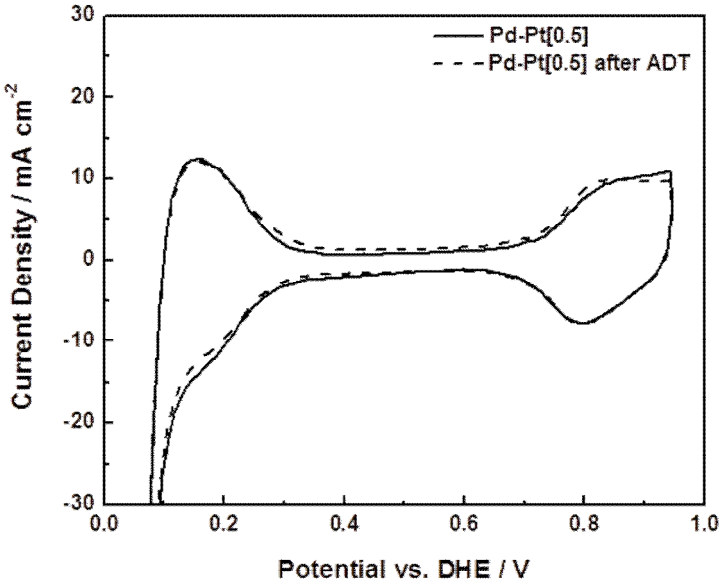

Fig. 3.11. Cyclic voltammograms of Pd-Pt[0.5] before and after ADT.

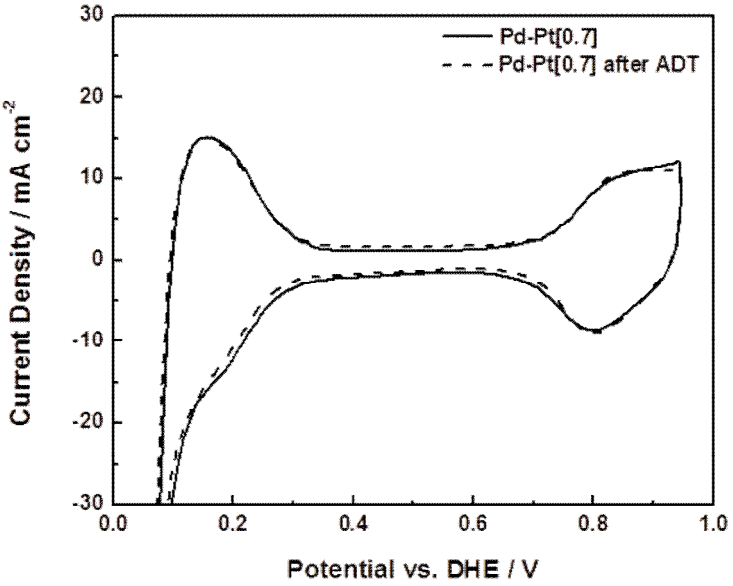

Fig. 3.12. Cyclic voltammograms of Pd-Pt[0.7] before and after ADT.

Table 3.2. The ESAs of Pt MEA, Pd-Pt[0.5], and Pd-Pt[0.7] before and After ADT.

	Pt MEA		Pd-Pt[0.5]		Pd-Pt[0.7]	
	Before	**After**	**Before**	**After**	**Before**	**After**
S_{ESA} / $m^2 g^{-1}$	**33.1**	**26.9**	**24.3**	**23.0**	**29.6**	**28.3**
Decrement rate / %	-	**18.7**	-	**5.3**	-	**4.4**

3.4 High Resolution-Transmission Electron Microscopy Analysis of the MEAs after ADT

The mean particle size and size distribution of the catalysts were measured using HR-TEM. Fig. 3.13 and 3.14 show the HR-TEM images and the size distribution histogram of Pt/C after 50 h of ADT. The mean particle size is 4.94 nm which measured from 100 ea. nanoparticles in Fig. 3.13. As the results indicate, the particle size of Pt/C increases from 3.83 to 4.94 nm after 50 h of ADT. In HR-TEM images, some agglomerations of particles are found, which are not shown in fresh Pt/C. The increase in Pt particles size affects the loss of ESA measured in cyclic voltammetry as shown in Fig. 3. 10.

As stated in section 1.4, the degradation mechanism of Pt electrode is dissolution and particle growth of Pt. Wilson et al. suggested that the increase of Pt particle size in aged MEA was due to the crystallite migration in the gas phase sintering. They reported that Pt particles migrated on the carbon surface and aggregated to larger Pt particles, and this increase of particle size corresponded to the loss of active surface area.[97]

On the other hand, many studies proposed that the dissolution and re-deposition of Pt were a major mechanism of degradation of the Pt electrocatalyst in fuel cell system.[81, 82] Pt dissolution was increased with

potential in the region of 0.85-0.95 V. In this study, ADTs were performed in the region of 0.35 to OCV (approximately 0.9 V) and operating conditions were similar with other studies. These ADT operating conditions may correspond to the increase of Pt particle size.

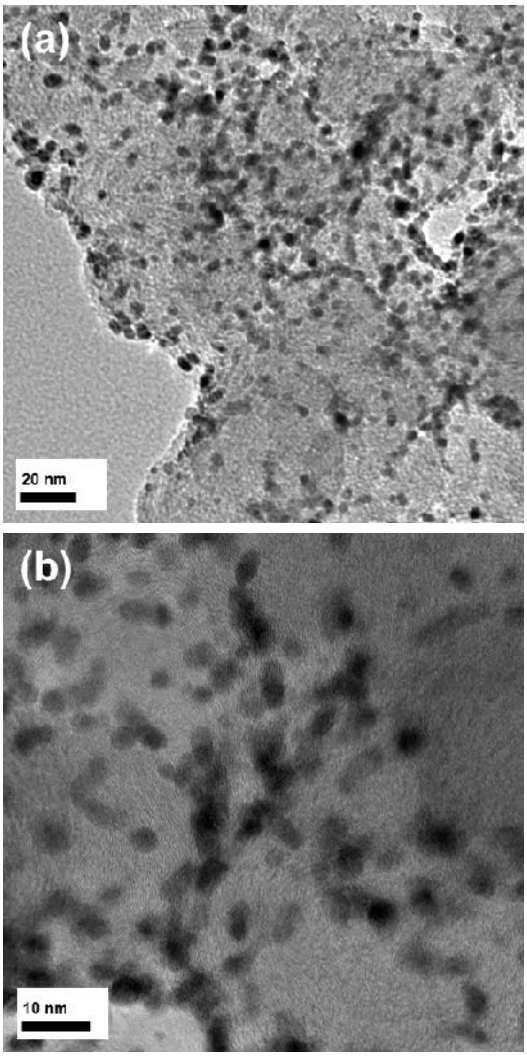

Fig. 3.13. HR-TEM images magnified (a) 120,000 times and (b) 300,000 times of Pt/C catalysts after ADT.

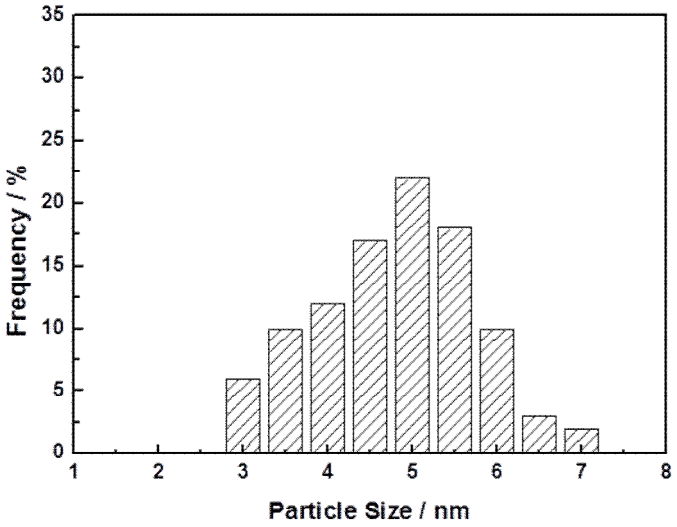

Fig. 3.14. The size distribution histogram of Pt/C catalysts after ADT.

Fig. 3.15 and Fig. 3.17 show the HR-TEM images of Pd-Pt[0.5]/C and Pd-Pt[0.7]/C after ADT. The corresponding size distribution histograms are shown in Fig 3.16 and 3.18. The mean particle size of Pd-Pt[0.5]/C and Pd-Pt[0.7]/C was 4.91 and 4.73 nm, which were measured from 100 ea. nanoparticles in the HR-TEM images. Increasing values of mean particle size were relatively smaller than that of Pt/C as cathode catalysts used in aged MEA.

In the case of Pt metal alloy catalysts, both Pt and the non-precious metal particles are dissolved. And the dissolved Pt redeposits on the surface of the catalyst particles. The dissolution of non-precious metal and increase of particle size have effect on the decrease of the performance. Popov and coworkers suggested that the main cause for the decay of catalytic activity for the Pt metal alloy catalyst was the metal dissolution, which indicated a different mechanism in the decay of catalytic activity for pure Pt catalysts.[86, 87] In their studies about PtNi/C and PtCo/C, the increase in the particle size of the Pt metal alloy catalysts was negligible after ADT. On the other hand, the decrement rates of catalytic activities for Pt metal alloy catalysts were approximately 50% after the ADT, which corresponded to the dissolution of non-precious metal. Other studies about Pt metal alloy catalyst also reported dissolution of non-precious metal and decrease of catalytic activity after

ADT.[41, 63]

However, core-shell catalyst and Pt metal alloy catalysts show different tendency of the performance degradation and changes in ESA. In this study, the curve shape of CV and ESA of Pd-Pt core-shell catalysts were similar before and after ADT, whereas those of Pt metal alloy catalysts were different due to the dissolution of non-precious metal according to prior studies. This result indicates that the degradation mechanism of Pd-Pt core-shell catalysts is different from that of pure Pt and Pt metal alloy catalysts.

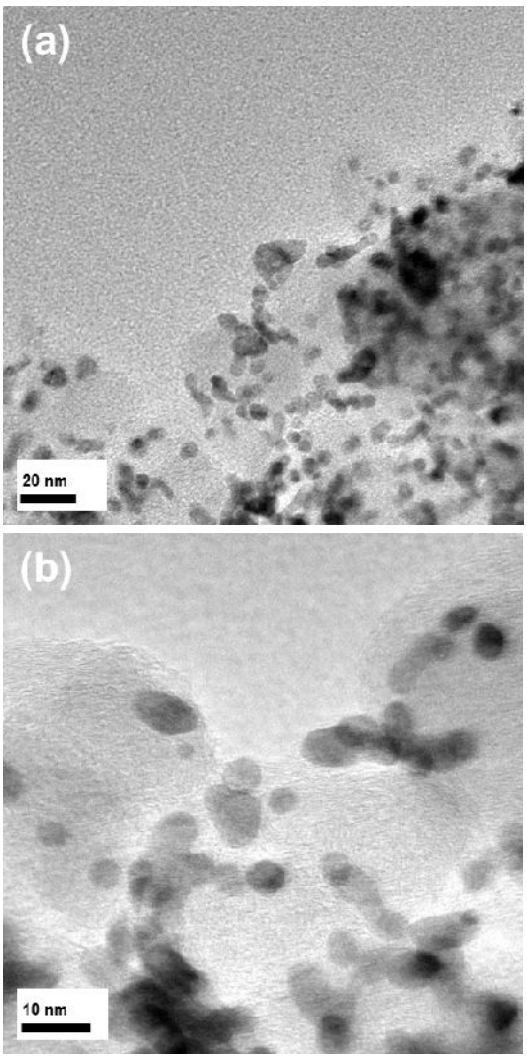

Fig. 3.15. HR-TEM images magnified (a) 120,000 times and (b) 300,000 times of Pd-Pt[0.5]/C catalysts after ADT.

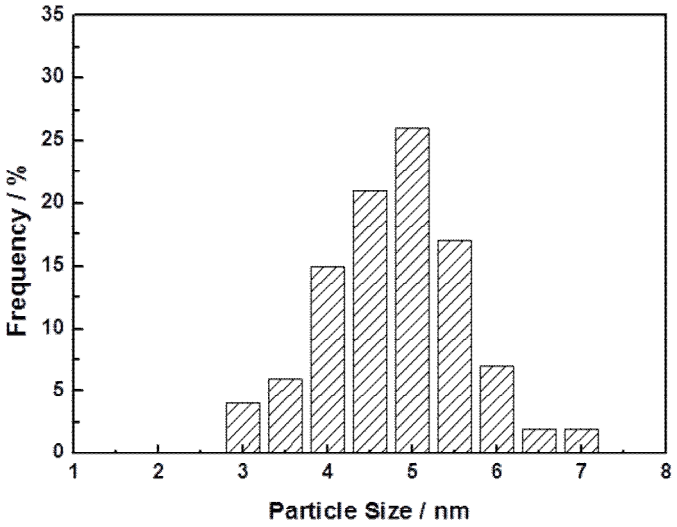

Fig. 3.16. The size distribution histogram of Pd-Pt[0.5]/C catalysts after ADT.

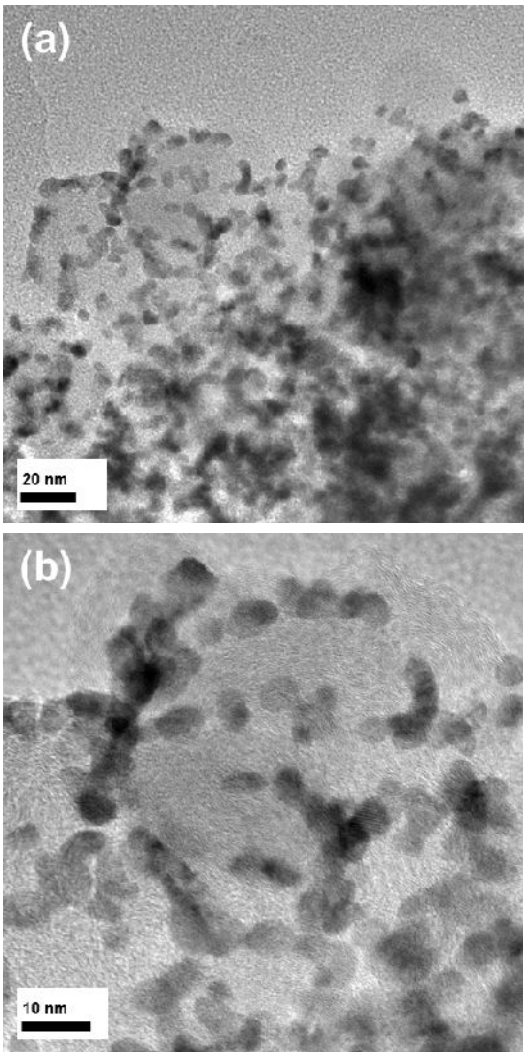

Fig. 3.17. HR-TEM images magnified (a) 120,000 times and (b) 300,000 times of Pd-Pt[0.7]/C catalysts after ADT.

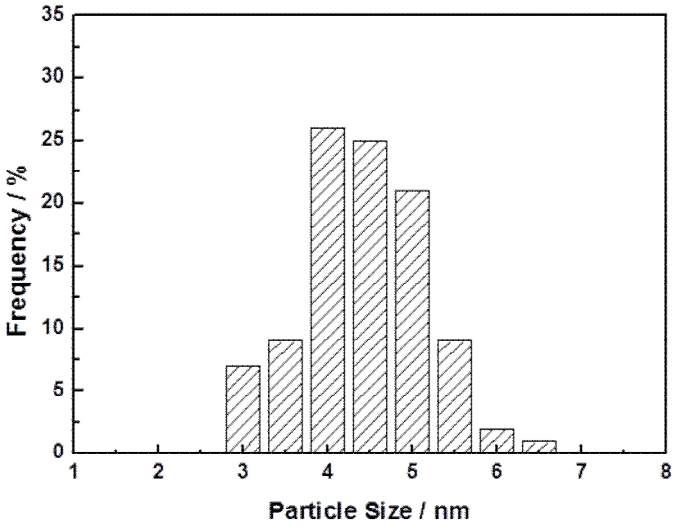

Fig. 3.18. The size distribution histogram of Pd-Pt[0.7]/C catalysts after ADT.

3.5 X-ray Diffraction Analysis of MEAs

X-ray diffraction (XRD) analysis was carried out on state of CCM as like a film. Fig. 3.19, 3.20, and 3.21 show the XRD patterns of the commercial Pt/C and synthesized Pd-Pt[0.5]/C and Pd-Pt[0.7]/C catalysts before and after ADT, respectively. The dashed line represents the peak position of initial Pt. It is well known that Pt and Pd have typical FCC lattice structures, which have intrinsic peaks for (111), (200), and (220) planes, and they have a similar atom size and crystal structure. The diffraction peaks at 2θ values of 40, 47 and 67 are associated with the (111), (200) and (220) planes, respectively. In all cases, the XRD profiles of the Pd-Pt core-shell catalysts showed the main peaks of the FCC structure. The (220) peak was used to calculate the average particle size of catalysts with the Scherrer equation because the (111) and (200) peaks with broad C peaks overlap each other.

$$D = \frac{0.94 \cdot \lambda k_{\alpha 1}}{B_{(2\theta)} \cdot cos\theta_{\max}}$$

where $\lambda k_{\alpha 1}$ is the wavelength of X-ray (1.5418 Å), $\theta_{\max}$ is the angle at the peak maximum, and $\beta_{2\theta}$ is the width of the peak at half height. $\theta_{\max}$ and $\beta_{2\theta}$ were determined with OriginPro 7.0 program

As expected, mean crystallite size of Pt/C was increased from 3.76 to 5.01

nm after ADT, which were in good agreement with the results of HR-TEM analysis. And the increase of mean crystallite size of Pt corresponds to the loss of ESA in CV. In initial MEA, the mean crystallite size of Pd-Pt[0.5]/C and Pd-Pt[0.7]/C were 3.98 and 4.30 nm, respectively. After ADT, the mean crystallite size of Pd-Pt[0.5]/C and Pd-Pt[0.7]/C were 4.99 and 4.71 nm, which were also good accord with results of HR-TEM analysis. The size of Pd-Pt[0.7]/C increased only 0.4 nm while that of Pd-Pt[0.5]/C increased 1.0 nm.

(220) peaks of Pd-Pt[0.5] and Pd-Pt[0.7] were shifted to high theta position. As shown in Fig. 3.20 and 3.21, (220) peak positions of Pd-Pt[0.5]/C and Pd-Pt[0.7]/C before ADT were 67.66 and 67.60 °, respectively. After ADT, those of Pd-Pt[0.5]/C and Pd-Pt[0.7]/C were shifted to 67.93 and 67.76 ° and the shapes of peaks were asymmetric. This result indicated that Pd-Pt core-shell nanoparticles were collapsed during ADT and Pd-Pt[0.5]/C catalyst was more decayed than Pd-Pt[0.7]/C catalyst. Overall it is found that the deposition amount of Pt shell in the core-shell structure has effect on the degradation of core-shell catalyst. The mean crystallite sizes and (220) peak positions of samples obtained from the XRD after ADT are given in Table 3.3

Table 3.3. The peak position and mean crystallite size of Pd-Pt[0.5]/C, Pd-Pt[0.7]/C, and Pt/C after ADT.

Catalyst	Mean crystallite size / nm	Peak position (220)
Pt/C	**5.01**	**67.60**
PdPt[0.5]/C	**4.99**	**67.93**
PdPt[0.7]/C	**4.71**	**67.76**

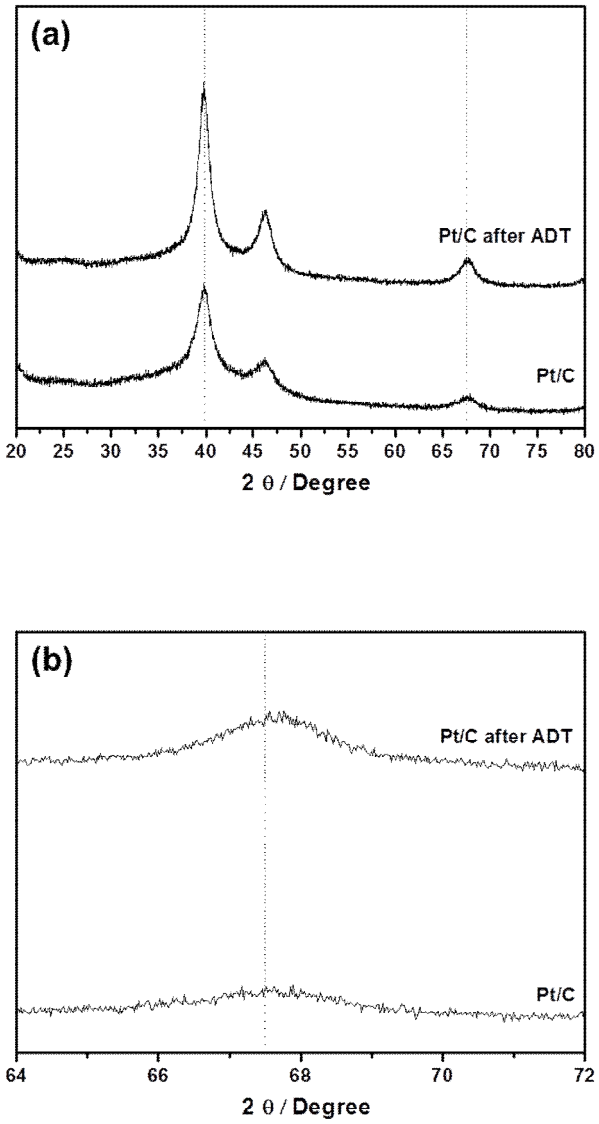

Fig. 3.19. (a) X-ray diffraction patterns and (b) peaks (220) of Pt/C before and after ADT.

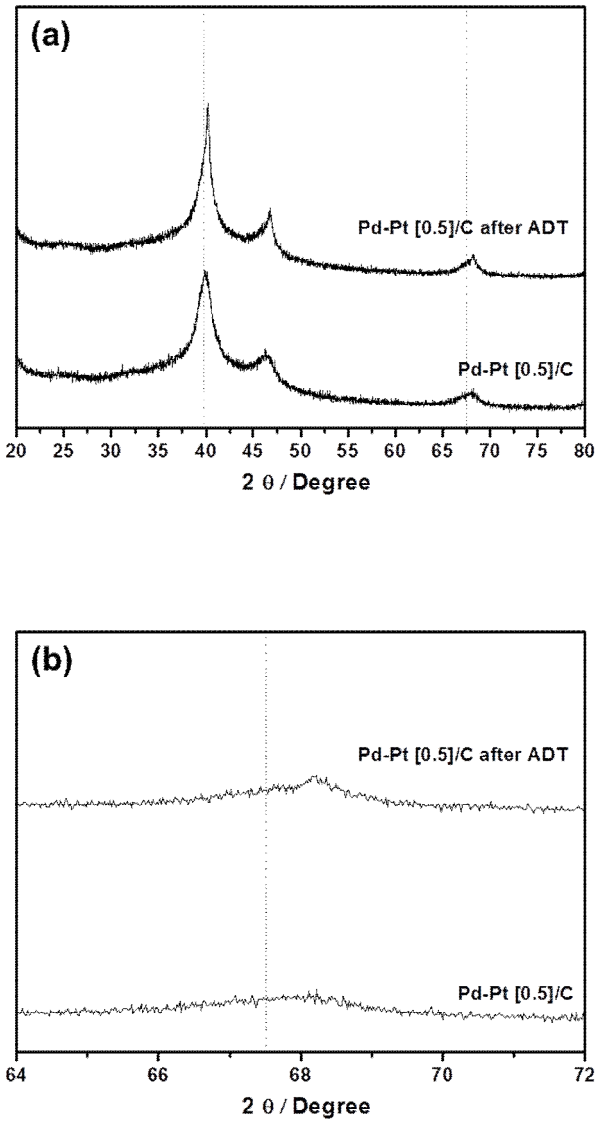

Fig. 3.20. (a) X-ray diffraction patterns and (b) peaks (220) of Pd-Pt[0.5]/C before and after ADT.

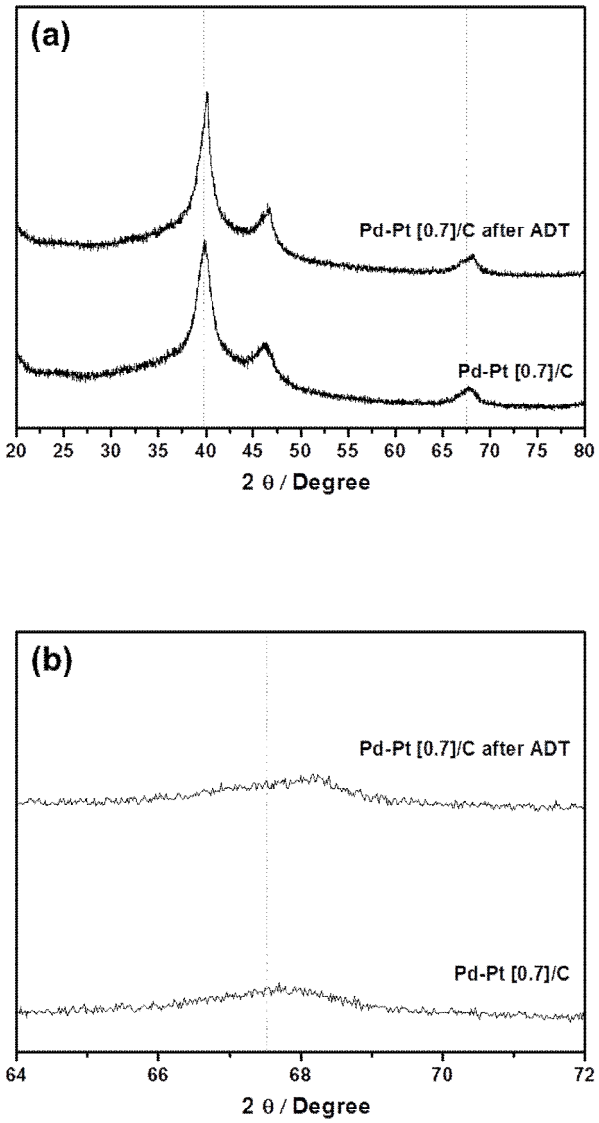

Fig. 3.21. (a) X-ray diffraction patterns and (b) peaks (220) of Pd-Pt[0.7]/C before and after ADT.

3.6 Field Emission-Scanning Electron Microscopy with Energy Dispersive X-ray Analysis of MEAs

FE-SEM analysis was performed to observe the changes in the structure of MEA before and after ADT. Fig. 3.22, 3.23 and 3.24 show the cross-section of Pt MEA, Pd-Pt[0.5] and Pd-Pt[0.7] before and after ADT, respectively. In some studies, the degradation of MEA structure has been reported after ADT. For instance, the mechanical stresses such as non-uniform contact pressure, fatigue from stresses by temperature and humidity might lead to thinning of membrane and crack in catalyst layer. In addition, the thinning of catalyst layer was caused by the carbon corrosion in catalyst layer. The degradation of MEA structure has effect on the decrease of the cell performance due to the increase of contact resistance and hydrogen crossover. However, in all cases, the structure of MEA was not changed significantly in this study.

On the other hand, some metal islands were observed in Pd-Pt[0.5] and Pd-Pt[0.7] after ADT as shown Fig 3.23(b) and 3.24(b). To confirm the element of the metal islands, energy dispersive X-ray analysis was performed. Fig. 3.25 and 3.26 show the elements distribution of Pd-Pt[0.5] and Pd-Pt[0.7] after ADT. In the membrane, the band of Pd element was appeared whereas there was not a significant signal coming from Pt. This result indicates that Pd in Pd-Pt core-shell catalyst may be dissolved whereas Pt is stable under

ADT.

The potential of Pd dissolution occurs at 0.92 V as following reaction:

$$Pd \rightarrow Pd^{2+} + 2e^{-}$$

which is lower than that of Pt (1.19 V). This indicates that Pd is more reactive than Pt, with a lower standard electrochemical potential. Therefore, Pd in Pd-Pt core-shell catalyst may be dissolved to Pd^{2+} and dissolved Pd diffuses through the imperfection in the Pt shell during ADT. It may diffuse into the ionomer phase and precipitate within the membrane. The precipitation was formed a Pd band as shown in Fig 3.25 and 3.26. This result is similar to the Pt band that resulted from the dissolution of Pt under ADT.[18] Adzic and coworkers reported that when Pt monolayer was placed on Pd substrate, the dissolution potential was relatively shifted and partial dissolution of Pd lead to the strengthened core-shell interaction.[98]

The elemental compositions of catalyst layer with Pd-Pt[0.5] and Pd-Pt[0.7] before and after ADT were characterized with energy dispersive X-ray analysis. Fig. 3.27 and 3.28 show the EDX spectrum of catalyst layer with Pd-Pt[0.5] and Pd-Pt[0.7] before and after ADT. The atomic ratios of initial Pd-Pt[0.5] and Pd-Pt[0.7], which corresponded to the expected values, were 66.87:33.13 and 62.80:37.20, respectively. After the ADT, the atomic ratios of Pd-Pt[0.5] and Pd-Pt[0.7] were 50.29:49.71 and 52.45:47.55, respectively.

This result also indicates the dissolution of Pd in Pd-Pt core-shell catalysts during ADT. And the Pd-Pt[0.7]/C is more stable than Pd-Pt[0.5]/C according to the changes in atomic ratio of catalysts before and after ADT. The bulk metal atomic ratios determined from EDX are shown in Table 3.4

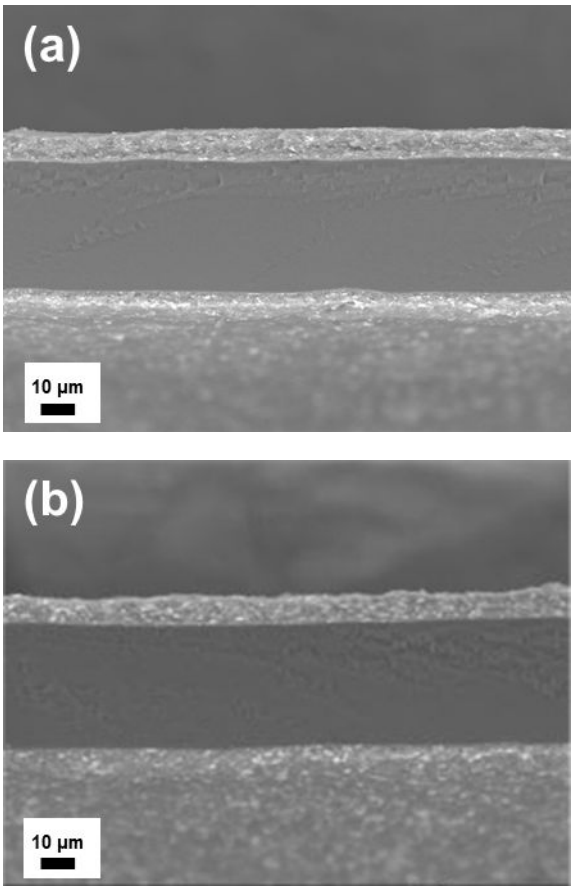

Fig. 3.22. The cross-section of Pt MEA (a) before and (b) after ADT.

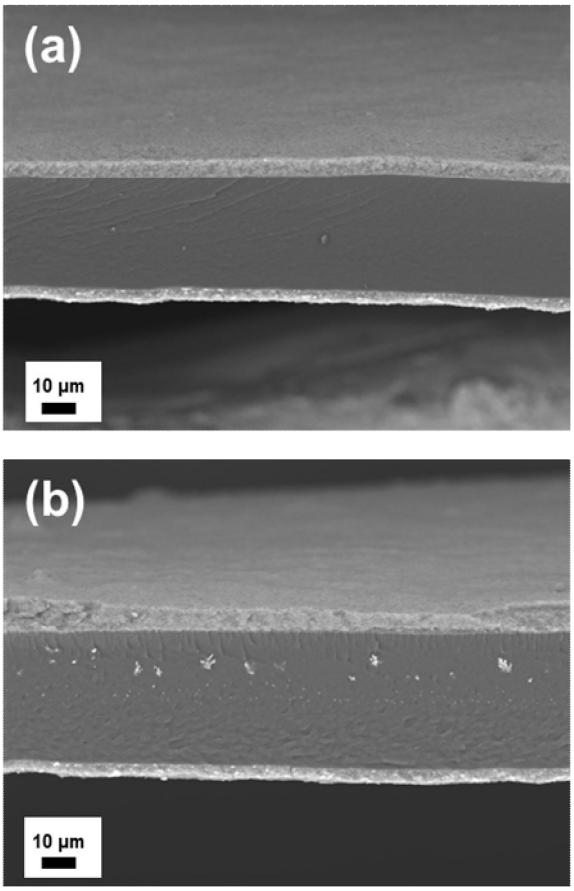

Fig. 3.23. The cross-section of Pd-Pt[0.5] (a) before and (b) after ADT.

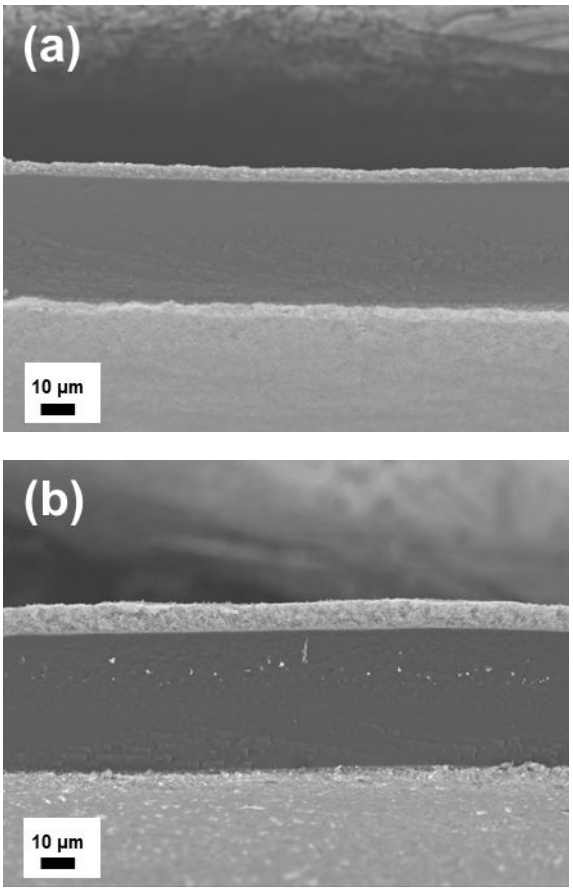

Fig. 3.24. The cross-section of Pd-Pt[0.7] (a) before and (b) after ADT.

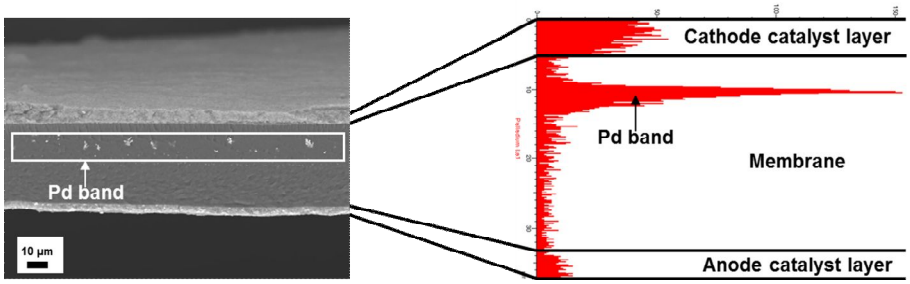

Fig. 3.25. The elements distribution of Pd-Pt[0.5] after ADT.

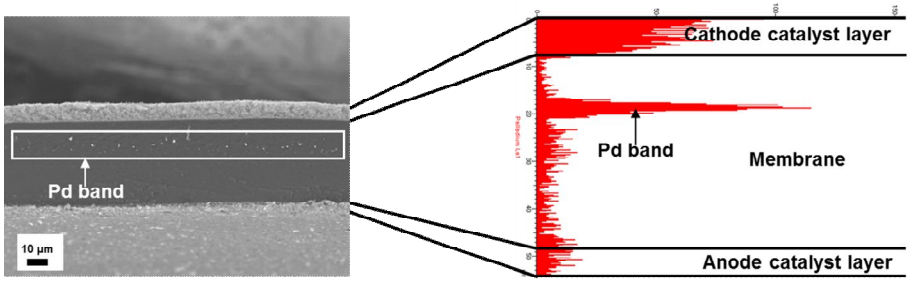

Fig. 3.26. The elements distribution of Pd-Pt[0.7] after ADT.

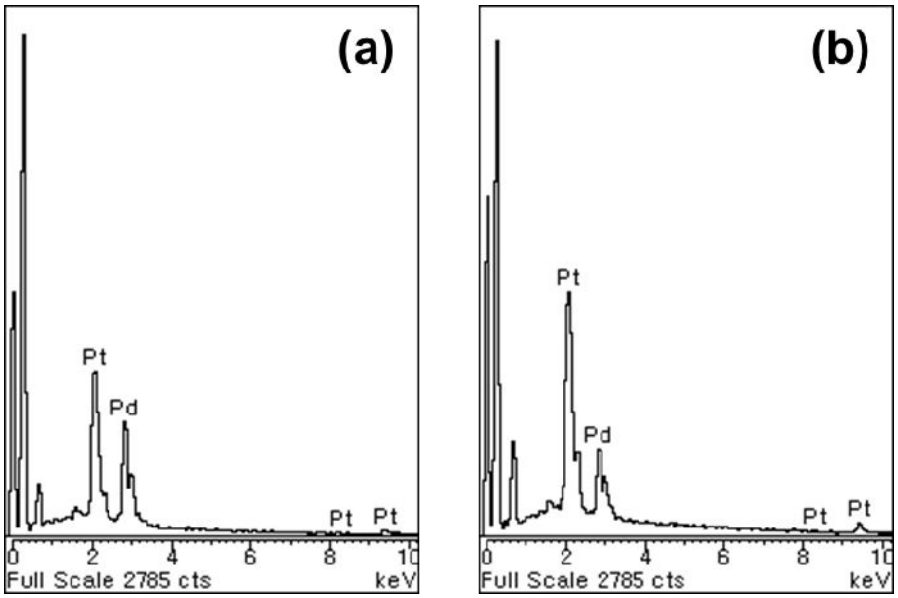

Fig. 3.27. The results of EDX with Pd-Pt[0.5] (a) before and (b) after ADT.

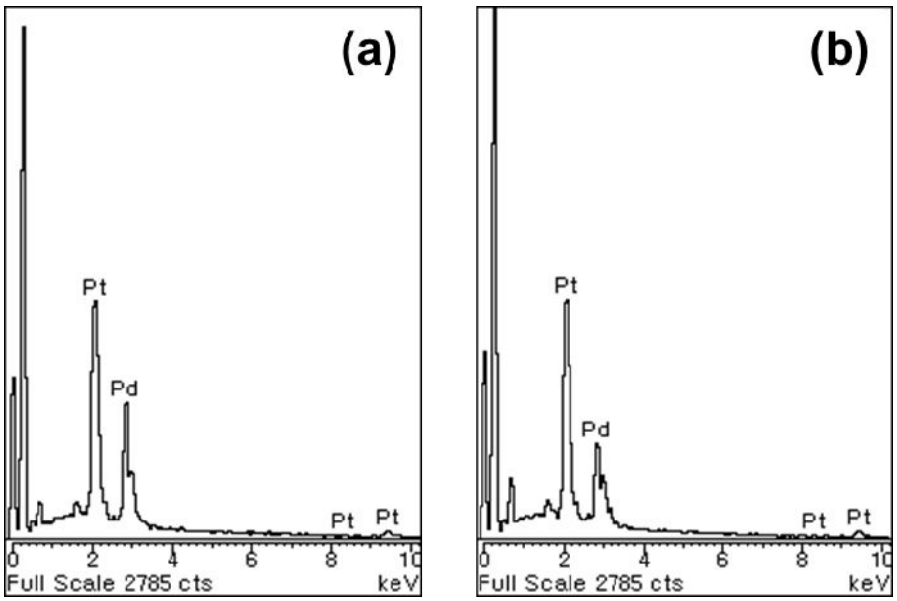

Fig. 3.28. The results of EDX with Pd-Pt[0.7] (a) before and (b) after ADT.

Table 3.4. The metal atomic ratios of Pd-Pt[0.5]/C and Pd-Pt[0.7]/C determined by EDX before and after ADT.

Catalyst	Composition / atom%	
	Pd	Pt
Initial PdPt [0.5]	66.87	33.13
PdPt [0.5] after ADT	50.29	49.71
Initial PdPt [0.7]	62.80	37.20
PdPt [0.7] after ADT	52.45	47.55

3.7 X-ray Photoelectron Spectroscopy of MEAs

X-ray photoelectron spectroscopy (XPS) is a powerful analysis tool widely used to characterize the chemical structure of materials. It has been used to study the degradation of catalyst layer and membrane in MEA due to its ability to determinate the chemical compositions of surfaces and recognize the chemical bonds from binding energies.

In order to confirm the degradation of Pd-Pt core-shell catalysts, XPS analysis was conducted in Pd-Pt[0.5] and Pd-Pt[0.7] before and after ADT. Fig. 3.29 shows the XPS spectra for the Pd3d core level spectra in Pd-Pt[0.5] before and after ADT. Specific information about binding energy of Pd-Pt[0.5] was arranged in Table 3.5. As shown Fig. 3.29, the spectrum could be deconvoluted into two pairs of doublets. The most intense doublet was characteristics of metallic Pd and weaker doublet could be assigned to Pd in oxidized forms. The two doublets for Pd3d were found at approximately 340.0 eV and 334.8 eV which corresponded to $Pd3d_{5/2}$ and $Pd3d_{3/2}$, respectively. After the ADT, the $Pd3d_{5/2}$ and $Pd3d_{3/2}$ were indicated at 340.2 eV and 334.9 eV which were similar with initial Pd-Pt[0.5]. However, the peak intensity of Pd decreased after ADT due to the Pd dissolution.

Fig. 3.30 shows the XPS spectra of the Pd-Pt[0.7] before and after ADT. The binding energy of Pd in initial Pd-Pt[0.7] is similar with that of Pd-

Pt[0.5]. The two doublets for Pd3d were found at approximately 340.2 eV and 334.9 eV which corresponded to $Pd3d_{5/2}$and $Pd3d_{3/2}$, respectively. After the ADT, the $Pd3d_{5/2}$ and $Pd3d_{3/2}$ were indicated at same binding energies. And the peak intensity of Pd decreased only slightly after ADT. This result indicated that the dissolution of Pd in Pd-Pt[0.7] was less than that of Pd-Pt[0.5]. The specific information about binding energy of Pd-Pt[0.7] also shown in Table 3.5.

The composition ratios of Pd-Pt[0.5]/C and Pd-Pt[0.7]/C catalysts before and after the ADT were analyzed by XPS. As shown in Table 3.6, the atomic ratios of initial Pd-Pt[0.5]/C and Pd-Pt[0.7]/C were 43.82:56.18 and 35.13:64.87, respectively. This result shows different compositions from EDX analysis because XPS result is representative of surface composition whereas EDX result represents bulk composition of catalysts. The surface composition of Pd-Pt[0.5]/C and Pd-Pt[0.7]/C catalysts show higher Pt content than the bulk composition because the catalysts are composed to Pd core and Pt shell structure. And the surface composition of Pd-Pt[0.7]/C catalysts shows higher Pt content than Pd-Pt[0.5]/C due to the different loading amount of Pt. After the ADT, the composition ratios of Pd-Pt[0.5]/C and Pd-Pt[0.7]/C catalysts were 39.19:60.81 and 33.71:66.29, respectively. The surface Pd:Pt compositions of catalyst after ADT were more Pt-rich than

the bulk Pd:Pt compositions. And this result shows the dissolution of Pd takes place in the Pd-Pt core-shell catalysts. The rate of change in composition indicates that Pd-Pt[0.7]/C catalyst is more stable than Pd-Pt[0.5]/C, which is good accordance with EDX result. This result suggests that stability of Pd-Pt core-shell catalysts may be affected by the amount of Pt deposition. The dissolution of Pd core is related to the Pt shell imperfection because the dissolved Pd diffuse through the imperfection in Pt shell.[98-100] The Pd core in Pd-Pt[0.7] was surrounded by larger amount of the Pt shell than that of Pd-Pt[0.5]. And this may have effect on the Pt shell imperfection.

XPS element mapping was conducted to visualize the difference in the Pd:Pt compositions of Pd-Pt[0.5]/C and Pd-Pt[0.7]/C catalysts before and after ADT. Fig. 3.31 and 3.32 show the XPS element mapping of Pd-Pt[0.5] and Pd-Pt[0.7] before and after ADT. In XPS element mapping, the Pd element is marked in red while the Pt is marked in blue. The images of Pd-Pt[0.5] and Pd-Pt[0.7] before ADT are similar. After the ADT, blue color is more apparent in the image of Pd-Pt[0.5] compared to that of initial Pd-Pt[0.5]. However, the image of Pd-Pt[0.7] after ADT is similar with that of initial Pd-Pt[0.7]. These results also indicate that the dissolution of Pd takes place in the Pd-Pt core-shell catalysts and Pd-Pt[0.7]/C catalyst is more

stable than Pd-Pt[0.5]/C. The XPS element mapping images correspond with the results of composition ratios in Table 3.6.

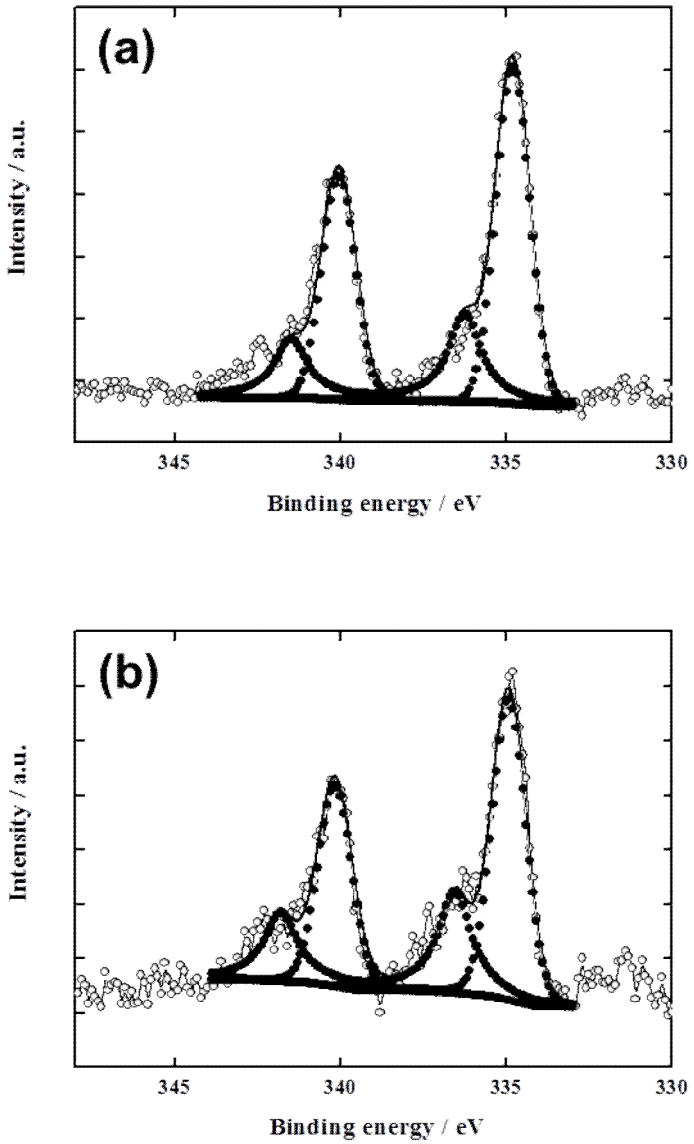

Fig. 3.29. Pd 3*d* X-ray photoelectron spectra of Pd-Pt[0.5]/C (a) before and (b) after ADT.

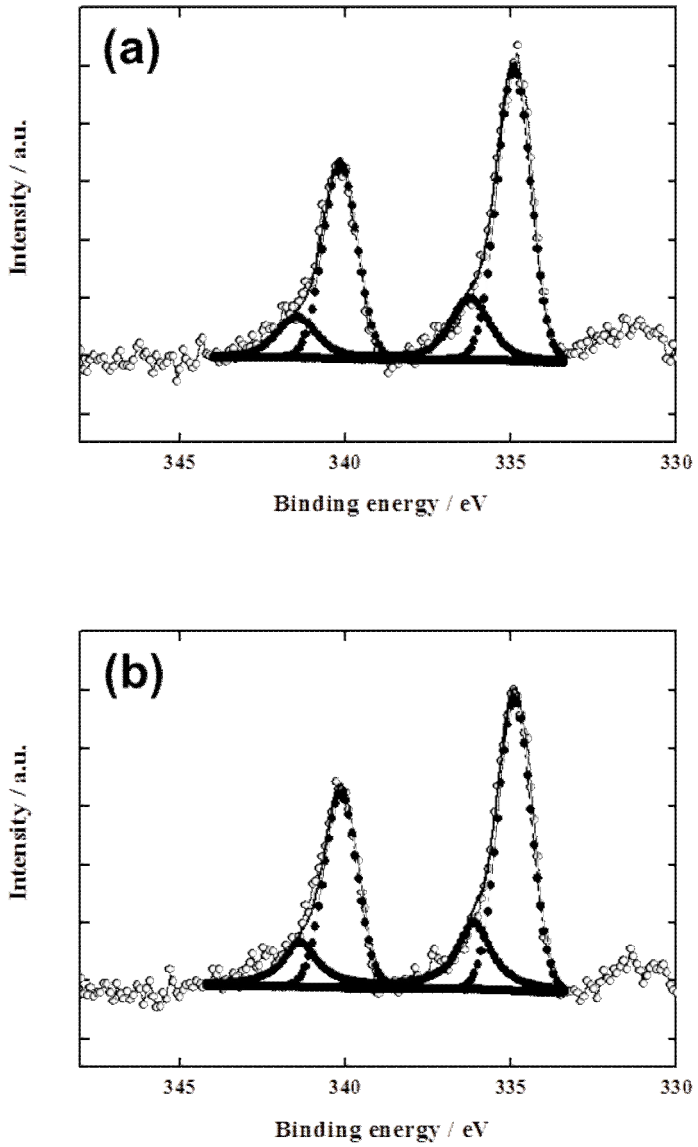

Fig. 3.30. Pd 3*d* X-ray photoelectron spectra of Pd-Pt[0.7]/C (a) before and (b) after ADT.

Table 3.5. XPS properties of Pd-Pt[0.5]/C and Pd-Pt[0.7]/C before and after ADT.

Catalyst	Species	Binding Energy / eV	
		Before	After
Pd-Pt[0.5]/C	Pd metal	340.0	340.2
	Pd metal	334.8	334.9
	PdO	341.5	341.8
	PdO	336.2	336.5
Pd-Pt[0.7]/C	Pd metal	340.2	340.2
	Pd metal	334.9	334.9
	PdO	341.5	341.5
	PdO	336.2	336.2

Table 3.6. The metal atomic ratios of Pd-Pt[0.5]/C and Pd-Pt[0.7]/C determined by XPS before and after ADT.

Catalyst	Composition / atom%	
	Pd	Pt
Initial PdPt [0.5]	43.82	56.18
PdPt [0.5] after ADT	39.19	60.81
Initial PdPt [0.7]	35.13	64.87
PdPt [0.7] after ADT	33.71	66.29

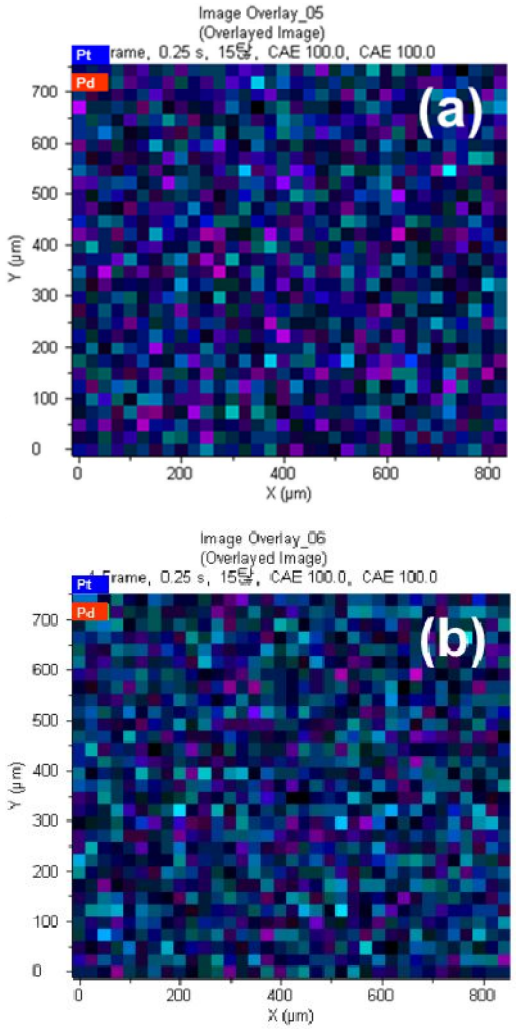

Fig. 3.31. XPS element mapping images of Pd-Pt[0.5] (a) before and (b) after ADT.

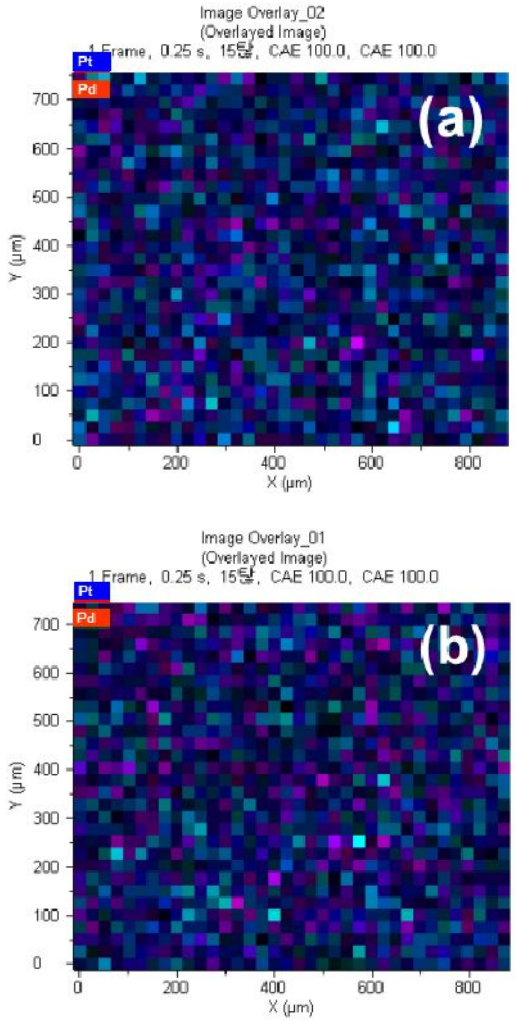

Fig. 3.32. XPS element mapping images of Pd-Pt[0.7] (a) before and (b) after ADT.

3.8 Summary of Results and Discussion

The carbon supported Pd-Pt core-shell catalysts were prepared for cathode in PEMFC. The structures of the synthesized Pd-Pt[0.5]/C, Pd-Pt[0.7]/C, and commercial Pt/C catalysts were determined by HR-TEM and XRD. The mean particle size of Pd-Pt[0.5]/C, Pd-Pt[0.7]/C and Pt/C nanoparticles was approximately 4.04, 4,37 and 3.83, respectively. The catalysts were well-dispersed on the surface of carbon support.

In the single cell performance under ADT, the Pt MEA showed the initial rapid decrease during 0-10 h. After 10 h under ADT, the performance of Pt MEA was slowly and gradually decreased. On the other hand, the performance of MEA with Pd-Pt core-shell was stable during initial 10 h. And then, the performance continuously declined after 10 h. The decrement rate of Pd-Pt[0.5] was higher than that of Pd-Pt[0.7] under ADT. In order to determine the changes in the ESA of the MEA before and after ADT, CV was performed. The ESA of Pt MEA reduced significantly whereas the decrement rate of ESA of Pd-Pt MEAs was negligible.

In the HR-TEM analysis, the particle sizes of Pd-Pt core-shell and Pt nanoparticles were increased after ADT. The increasing extent of Pd-Pt core-shell nanoparticles was smaller than that of Pt nanoparticles. In the results of XRD analysis, the mean crystallite size of Pd-Pt core-shell and Pt

nanoparticles was increased after ADT. This result is good accordance with HR-TEM analysis. The main peak positions of Pd-Pt core-shell catalyst were shifted and the shapes of peak were asymmetric. These results suggested that the core-shell catalysts were decayed during ADT. In the results of FE-SEM analysis in MEA, the Pd metal islands were observed in the MEA with Pd-Pt core-shell catalysts. This result indicates that Pd in Pd-Pt core-shell catalyst may be dissolved under ADT. The elemental compositions of catalyst layer with Pd-Pt[0.5]/C and Pd-Pt[0.7]/C before and after ADT were characterized with energy dispersive X-ray analysis. The EDX results also indicate the dissolution of Pd during ADT. And the Pd-Pt[0.7]/C catalyst was more stable than Pd-Pt[0.5]/C catalyst according to the changes in atomic ratio of catalysts before and after ADT. To confirm the degradation of Pd-Pt core-shell catalyst, XPS analysis was performed in MEA with Pd-Pt core-shell catalyst before and after ADT. In all cases, the binding energies of Pd3d were similar. However, the composition ratios of Pd and Pt were changed before and after ADT. The changes in composition of Pd and Pt were caused by the dissolution of Pd in Pd-Pt core-shell catalyst.

In the case of Pt MEA, the initial rapid decrease of performance corresponded to the loss of ESA. In the structure analysis, the mean particle size of Pt was significantly increased and this result had effect on the loss of

ESA. In the case of Pd-Pt core-shell catalysts, the initial decrease of performance with Pd-Pt core-shell was smaller than that of Pt. The core-shell structure may affect the stability of the Pt shell, which is consistent with the results of ESA calculated from CV. However, after 10 h under ADT, the performance of the MEA with Pd-Pt core-shell catalyst declined continuously. The decrease of the performance is related to the dissolution of Pd in Pd-Pt core-shell catalyst, which has effect on the activity of Pd-Pt core-shell catalyst. In the case of Pd-Pt[0.5]/C and Pd-Pt[0.7]/C, the performance of Pd-Pt[0.7] is more stable than Pd-Pt[0.5], which may be caused by the amount of Pt deposition. This result is good accordance with the results of XRD and change in atomic ratio before and after ADT.

Chapter 4. Conclusions

The performance degradation of Pd-Pt core-shell and Pt/C catalysts were evaluated by the ADT using load cycling. To apply the single cell, MEAs were fabricated with Pd-Pt core-shell and Pt/C as cathode catalysts. Electrochemical and structure analyses were conducted to understand the degradation characteristics of Pd-Pt core-shell and Pt/C catalysts.

In the current voltage characteristics, the initial performance of Pd-Pt[0.5] and Pd-Pt[0.7] were 440 and 400 mA cm^{-2} at 0.7 V, which were comparable to that of Pt/C. After ADT, the performance of Pt MEA, Pd-Pt[0.5], and Pd-Pt[0.7] were decreased approximately 39, 45, and 40%, respectively. The Pt MEA showed the initial rapid decrease of performance during 0-10 h. On the other hand, the performances of the MEAs with Pd-Pt core shell catalysts were stable. After the 10 h, the performance of Pt MEA was slowly and gradually declined. However, the performances of MEA with Pd-Pt core-shell catalysts were continuously declined during the ADT. The decreasing rates of ESA of Pt, Pd-Pt[0.5], and Pd-Pt[0.7] MEA were 18.7 %, 5.3 %, and 4.4 %, respectively. This result indicated that the decrease of performance in Pt MEA was associated with the loss of ESA.

In structure analysis, the particle sizes of Pd-Pt core-shell and Pt/C catalysts

were increased after ADT. And the increasing extent of Pd-Pt core-shell nanoparticles was smaller than that of Pt nanoparticles. The growth of Pt particle had effect on the loss of ESA. The results of XPS and FE-SEM indicated that Pd in Pd-Pt core-shell catalyst was dissolved and the dissolved Pd formed Pd band. The continuous decrease of performance in Pd-Pt core-shell MEA was related to the Pd dissolution.

In the case of Pd-Pt[0.5]/C and Pd-Pt[0.7]/C, the performance of Pd-Pt[0.7] is more stable than Pd-Pt[0.5], which may be affected by the amount of Pt deposition. This result is good accordance with the results of XRD and the change in atomic ratio before and after ADT.

These results indicated that the degradation tendency of pure Pt and Pd-Pt core-shell catalysts are different. The major cause of degradation in pure Pt is the loss of ESA, whereas that in Pd-Pt core-shell catalyst is dissolution of Pd core. And the shell perfection is the important factor to enhance the durability in core-shell catalyst. It suggested that development of synthesis method which can improve the shell perfection can be the topics for future studies.

References

1. R. O'Hayre, S. W. Cha, W. Colella, and F. B. Prinz, "Fuel cell fundamentals", John Wiley & Sons, New York, 2006.
2. J. Larminie and A. Dicks, "Fuel cell systems explained", John Wiley & Sons, 2000.
3. F. Barbir, "PEM fuel cells: theory and practice", Elsevier Academic Press, San Diego, 2005.
4. A. Biyikoglu, "Review of proton exchange membrane fuel cell models", *Int. J. Hydrogen Energy*, **30**, 1181-1212 (2005)
5. D. P. Wilkinson, J. St-Pierre, in: W. Vielstich, A. Lamm, and H. A. Gasteiger (Eds.), "Handbook of fuel cells: fundermentals, technology and applications", vol. 3, John Wiley & Sons, 2003.
6. C. Wieser, "Novel polymer electrolyte membranes for automotive applications – requirements and benefits", *Fuel cells*, **4**, 245-250 (2004)
7. D. Dunwoody and J. Leddy, "Proton exchange membranes: the view forward and back", *Electrochem. Soc. Interf.*, **14**, 37-39 (2005)
8. A. Collier, H. Wang, X. Yuan, J. Zhang, and D. P. Wilkinson, "Degradation of polymer electrolyte membranes", *Int. J. Hydrogen Energy*, **31**, 1838-1854 (2006)
9. N. Rajalakshmi and K. S. Dhathathreyan, "Present trends in fuel cell

technology development", Nova Publishers, 2008.

10. I. fishtik, C. A. Callaghan, J. D. fehribach, and R. Datta, "A reaction route graph analysis of the electrochemical hydrogen oxidation and evolution reactions", *J. Electroanal. Chem.*, **576**, 57-63 (2005)
11. E. B. Yeager, "Electrocatalysts for O_2 reduction", *Electrochim. Acta*, **29**, 1527-1537 (1984)
12. V. S. Bagotskii, M. R. Tarasevich, and V. Y. Filinovskii, "Calculation of the kinetic parameters of conjugated reactions of oxygen and hydrogen peroxide", *Elektrokhimiya*, **5**, 1218-1226 (1969)
13. V. S. Bagotskii, M. R. Tarasevich, and V. Y. Filinovskii, "Accounting for the adsorption stage in a calculation of the kinetic parameters of oxygen and hydrogen peroxide reactions", *Elektrokhimiya*, **8**, 84-87 (1972)
14. S. Hommura, K. Kawahara, T. Shimohira, and Y. Teraoka, "Development of a method for clarifying the perfluorosulfonated membrane degradation mechanism in a fuel cell environment", *J. Eletrochem. Soc.*, **155**, A29-A33 (2008)
15. X.Yang, F. Zhang, A. Lubawy, and C. Wang, "Visualization of liquid water transport in a PEFC", *Electrochem. Solid-State Lett.*, **7**, A408-A411 (2004)

16. S. Chalk and J. Miller, “Key challenges and recent progress in batteries, fuel cells, and hydrogen storage for clean energy systems”, *J. Power Sources*, **159**, 73-80 (2006)
17. M. S. Wilson, J. A. Valerio, and S. J. Gottesfeld, “Low platinum loading electrodes for polymer electrolyte fuel cells fabricated using thermoplastic ionomers”, *Electrochim. Acta,* **40**, 355-363 (1995)
18. H. A. Gasteiger, S. S. Kocha, B. Sompalli, and F. T. Wagner, “Activity benchmarks and requirements for Pt, Pt-alloy, and non-Pt oxygen reduction catalysts for PEMFCs”, *Appl. Catal. B: Environ.*, **56**, 9-35 (2005)
19. J. Zhao, A. Sarkar, and A. Manthiram, “Synthesis and characterization of Pd-Ni nanoalloy electrocatalysts for oxygen reduction reaction in fuel cells”, *Electrochim. Acta,* **55**, 1756-1765 (2010)
20. K. Sawai and N. Suzuki, “Highly active nonplatinum catalyst for air cathodes”, *J. Electrochem. Soc.*, **151**, A2132-A2137 (2004)
21. H. Zhong, H. Zhang, G. Liu, Y. Liang, J. Hu, and B. Yi, “A novel non-noble electrocatalysts for PEM fuel cell based on molybdenum nitride”, *Electrochem. Commun.*, **8**, 707-712 (2006)
22. T. Toda, H. Igarashi, H. Uchida, and M. Watanabe, “Enhancement of the electroreduction of oxygen on Pt alloys with Fe, Ni, and Co”, *J.*

Electrochem. Soc., **146**, 3750-3756 (1999)

23. U. A. Paulus, A. Wokaun, and G. G. Scherer, "Oxygen reduction on carbon-supported Pt-Ni and Pt-Co alloy catalysts", *J. Phys. Chem. B*, **106**, 4181-4191 (2002)
24. H. Yang, N. Alonso-Vante, J. M. Leger, and C. Lamy, "Tailoring, structure, and activity of carbon-supported nanosized Pt-Cr alloy electrocatalysts for oxygen reduction in pure and methanol-containing electrolytes", *J. Phys. Chem. B*, **108**, 1938-1947 (2004)
25. F. Liu and C. Y. Wang, "Optimization of cathode catalyst layer for direct methanol fuel cells: Part I. Experimental investigation", *Electrochim. Acta*, **52**, 1417-1425 (2006)
26. D. You, Y. Lee, H. Cho, J. H. Kim, C. Park, G. Lee, K. Y. Park, and J. Y. Park, "High performance membrane electrode assemblies by optimization of coating process and catalyst layer structure in direct methanol fuel cell", *Int. J. Hydrogen Energy*, **36**, 5096-5103 (2011)
27. J. Cao, M. Chen, J. Chen, S. Wang, Z. Zou, Z. Li, D. L. Akins, and H. Yang, "Double microporous layer cathode for membrane electrode assembly of passive direct methanol fuel cells", *Int. J. Hydrogen Energy*, **35**, 4622-4629 (2010)
28. J. H. Cho, J. M. Kim, J. Prabhuram, S. Y. Hwang, D. J. Ahn, H. Y. Ha,

and S. K. Kim, “Fabrication and evaluation of membrane electrode assemblies by low-temperature decal methods for direct methanol fuel cells”, *J. Power Sources*, **187**, 378-386 (2009)

29. M. S. Saha, D. K. Paul, B. A. Peppley, and K. Karan, “Fabrication of catalyst-coated membrane by modified decal transfer technique”, *Electrochem. Commun*., **12**, 410-413 (2010)
30. H. Tang, S. Wang, M. Pan, S. P. Jiang, and Y. Ruan, “Performance of direct methanol fuel cells prepared by hot-pressed MEA and catalyst-coated membrane (CCM)”, *Electrochim. Acta*, **52**, 3714-3718 (2007)
31. C. K. Withham, W. Chun, T. I. Valdez, and S. R. Narayanan, “Performance of direct methanol fuel cells with sputter-deposited anode catalyst layers”, *Electrochem. Solid-State Lett*., **3**, 497-500 (2000)
32. H. S. Park, Y. H. Cho, Y. H. Cho, C. R. Jung, J. H. Jang, and Y. E. Sung, “Performance enhancement of PEMFC through temperature control in catalyst layer fabrication”, *Electrochim. Acta*, **53**, 763-767 (2007)
33. T. V. Reshetenko, H. T. Kim, and H. J. Kweon, “Cathode structure optimization for air-breathing DMFC by application of pore-forming agents”, *J. Power Sources*, **171**, 433-440 (2007)

34. C. Y. Chen and C. S. Tsao, “Characterization of electrode structures and the related performance of direct methanol fuel cells”, *Int. J. Hydrogen Energy*, **31**, 391-398 (2006)

35. Z. Wei, S. Wang, B. Yi, J. Liu, L. Chen, W. Zhou, W. Li, and Q. Xin, “Influence of electrode structure on the performance of a direct methanol fuel cell”, *J. Power Sources*, **106**, 364-369 (2002)

36. J. Zhao, X. He, L. Wang, J. Tian, C. Wan, and C. Jiang, “Addition of NH_4HCO_3 as pore-former in membrane electrode assembly for PEMFC”, *Int. J. Hydrogen Energy*, **32**, 380-384 (2007)

37. C. S. Kong, D. Y. Kim, H. K. Lee, Y. G. Shul, and T. H. Lee, “Influence of pore-size distribution of diffusion layer on mass-transport problems of proton exchange membrane fuel cells”, *J. Power Sources*, **108**, 185-191 (2002)

38. M. Uchida, Y. Aoyama, N. Eda, and A. Ohta, “Investigation of the microstructure in the catalyst layer and effects of both perfluorosulfonate ionomer and PTFE-loaded carbon on the catalyst layer of polymer electrolyte fuel cells”, *J. Electrochem. Soc.*, **142**, 4143-4149 (1995)

39. E. Antolini, “Palladium in fuel cell catalysis”, *Energy Environ. Sci.*, **2**, 915-931 (2009)

40. O. Savadogo, K. Lee, K. Oishi, S. Mitsushima, N. Kamiya, and K. I. Ota, "New palladium alloys catalyst for the oxygen reduction reaction in an acid medium", *Electrochem. Commun*., **6**, 105-109 (2004)
41. J. Zhao, K. Jarvis, P. Ferreira, and A. Manthiram, "Performance and stability of Pd-Pt-Ni nanoalloy electrocatalysts in proton exchange membrane fuel cells", *J. Power Sources*, **196**, 4515-4523 (2011)
42. Y. Tang, H. Zhang, H. Zhong, T. Xu, and H. Jin, "Carbon-supported Pd-Pt cathode electrocatalysts for proton exchange membrane fuel cells", *J. Power Sources*, **196**, 3523-3529 (2011)
43. J. L. Fernandez, D. A. Walsh, and A. J. Bard, "Thermodynamic guidelines for the design of bimetallic catalysts for oxygen electroreduction and rapid screening by scanning electrochemical miscroscopy. M-Co (M: Pd, Ag, Au)", *J. Am. Chem. Soc*., **127**, 357-365 (2005)
44. M. H. Shao, K. Sasaki, and R. R. Adzic, "Pd−Fe nanoparticles as electrocatalysts for oxygen reduction", *J. Am. Chem. Soc*., **128**, 3526-3527 (2006)
45. J.L. Fernandez, V. Raghuveer, A. Manthiram, and A.J. Bard, "Pd−Ti and Pd−Co−Au electrocatalysts as a replacement for platinum for oxygen reduction in proton exchange membrane fuel cells", *J. Am.*

Chem. Soc., **127**, 13100-13101 (2005)

46. S. A. Grigoriev, E. K. Lyutikova, S. Martemianov, and V. N. Fateev, "On the possibility of replacement of Pt by Pd in a hydrogen electrode of PEM fuel cells", *Int. J. Hydrogen Energy*, **32**, 4438-4442 (2007)
47. J. Barbier, E. Lamy, and O. Outiki, "Platinum-palladium catalysts for hydrogen fuel cell electrodes", *React. Kinet. Catal. Lett.*, **18**, 127-132 (1981)
48. D. J. Ham, C. Park, G. H. Bae, S. Han, K. Kwon, S. A. Jin, H. Chang, S. H. Choi, and J. S. Lee, "Palladium-nickel alloys loaded on tungsten carbide as platinum-free anode electrocatalysts for polymer electrolyte membrane fuel cells", *Chem. Commun.*, **47**, 5792-5794 (2011)
49. Y. H. Cho, B. Choi, Y. H. Cho, H. S. Park, and Y. E. Sung, "Pd-based PdPt(19:1)/C electrocatalyst as an electrode in PEM fuel cell", *Electrochem. Commun.*, **9**, 378-381 (2007)
50. Y. H. Cho, Y. H. Cho, J. W. Lim, H. Y. Park, N. Jung, M. Ahn, H. Choe, and Y. E. Sung, "Performance of membrane electrode assemblies using PdPt alloy as anode catalysts in polymer electrolyte membrane fuel cell", *Int. J. Hydrogen Energy*, **37**, 5884-5890 (2012)
51. D. C. Papageorgopoulos, M. Keijzer, J. Veldhuis, and F. A. De Bruijin, "CO tolerance of Pd-rich platinum palladium carbon-supported

electrocatalysts: proton exchange membrane fuel cell applications", *J. Electrochem. Soc.*, **149**, A1400-A1404 (2002)

52. A. C. Garcia, V. A. Paganin, and E. A. Ticianelli, "CO tolerance of PdPt/C and PdPtRu/C anodes for PEMFC", *Electrochim. Acta*, **53**, 4309-4315 (2008)
53. F. Alcaide, G. Alvarez, P. L. Cabot, O. Miguel, and A. Querejeta, "Performance of carbon-supported PtPd as catalyst for hydrogen oxidation in the anodes of proton exchange membrane fuel cells", *Int. J. Hydrogen Energy*, **35**, 11634-11641 (2010)
54. S. J. Yoo, H. Y. Park, T. Y. Jeon, I. S. Park, Y. H. Cho, and Y. E. Sung, "Promotional effect of palladium on the hydrogen oxidation reaction at a PtPd alloy electrode", *Angew. Chem. Int. Ed.*, **47**, 9307-9310 (2008)
55. S. Tominaka, T. Momma, and T. Osaka, "Electrodeposited Pd-Co catalyst for direct methanol fuel cell electrodes: preparation and characterization", *Electrochim. Acta*, **53**, 4679-4686 (2008)
56. X. Li, Q. Huang, Z. Zou, B. Xia, and H. Yang, "Low temperature preparation of carbon-supported PdCo alloy electrocatalysts for methanol-tolerant oxygen reduction reaction", *Electrochim. Acta*, **53**, 6662-6667 (2008)

57. W. M. Wang, D. Zheng, C. Du, Z. Q. Zou, X. Q. Zhang, B. J. Xia, H. Yang, and D.L. Akins, "Carbon-supported Pd-Co bimetallic nanoparticles as electrocatalysts for the oxygen reduction reaction", *J. Power Sources*, **167**, 243-249 (2007)

58. K. Lee, O. Savadogo, A. Ishihara, S. Mitsushima, N. Kamiya, and K.I. Ota, "Methanol-tolerant oxygen reduction electrocatalysts based on Pd-3d transition metal alloys for direct methanol fuel cells", *J. Electrochem. Soc.*, **153**, A20-A24 (2006)

59. W. M. Wang, Q. H. Huang, J. Y. Liu, Z. Q. Zou, Z. L. Li, and H. Yang, "One-step synthesis of carbon-supported Pd–Pt alloy electrocatalysts for methanol tolerant oxygen reduction", *Electrochem. Commun.*, **10**, 1396-1399 (2008)

60. W. He, J.Y. Liu, Y.J. Qiao, Z.Q. Zou, X.G. Zhang, D.L. Akins, and H. Yang, "Simple preparation of Pd–Pt nanoalloy catalysts for methanol-tolerant oxygen reduction", *J. Power Sources*, **195**, 1046-1050 (2010)

61. H. Wang, C. Xu, F. Cheng, M. Zhang, S. Wang, and S. P. Jiang, "Pd/Pt core-shell nanowire arrays as highly effective electrocatalysts for methanol electrooxidation in direct methanol fuel cells", *Electrochem. Commun.*, **10**, 1575-1578 (2008)

62. A. N. Golikand, E. Lohrasbi, M. G. Maragheh, and M. Asgari,

"Carbon nano-tube supported Pt-Pd as methanol-resistant oxygen reduction electrocatalyts for enhancing catalytic activity in DMFCs", *J. Appl. Electrochem*., **39**, 2421-2431 (2009)

63. J. Zhao and A. Manthiram, "Preleached Pd-Pt-Ni and binary Pd-Pt electrocatalysts for oxygen reduction reaction in proton exchange membrane fuel cells", *Appl. Catal. B*, **101**, 660-668 (2011)
64. V. Parry, G. Berthome, J. C. Joud, O. Lemaire, and A. A. Franco, "XPS investigations of the proton exchange membrane fuel cell active layers aging: characterization of the mitigating role of an anodic CO contamination on cathode degradation", *J. Power Sources*, **196**, 2530-2538 (2011)
65. F. A. de Bruijn, V. A. T. Dam, and G. J. M. Janssen, "Review: durability and degradation issues of PEM fuel cell components", *Fuel Cells*, **1**, 3-22 (2008)
66. S. Zhang, X. Yuan, J. N. C. Hin, and H. Wang, "A review of platinum-based catalyst layer degradation in proton exchange membrane fuel cells", *J. Power Sources*, **194**, 588-600 (2009)
67. S. Zhang, X. Yuan, H. Wang, W. Merida, H. Zhu, J. Shen, S. Wu, and J. Zhang, "A review of accelerate stress tests of MEA durability in PEM fuel cells", *Int. J. Hydrogen Energy*, **34**, 388-404 (2009)

68. Y. H. Cho, T. Y. Jeon, S. J. Yoo, K. S. Lee, M. Ahn, O. H. Kim, Y. H. Cho, J. W. Lim, N. Jung, W. S. Yoon, H. Choe, and Y. E. Sung, "Stability characteristics of Pt_1Ni_1/C as cathode catalysts in membrane electrode assembly of polymer electrolyte fuel cell", *Electrochim. Acta*, **59**, 264-269 (2012)

69. Y. H. Cho, J. W. Lim, Y. S. Kang, Y. H. Cho, O. H. Kim, N. H. Kwon, O. J. Kwon, W. S. Yoon, H. Choe, and Y. E. Sung, "The dependence of performance degradation of membrane electrode assembly on platinum loading in polymer electrolyte membrane fuel cell", *Int. J. Hydrogen Energy*, **37**, 2490-2497 (2012)

70. Z. Zhou, Z. Shao, X. Qin, X. Chen, Z. Wei, and B. Yi, "Durability study of Pt-Pd/C as PEMFC cathode catalyst", *Int. J. Hydrogen Energy*, **35**, 1719-1726 (2010)

71. J. Wu, X. Yuan, J. J. Martin, H. Wang, J. Zhang, J. Shen, S. Wu, and W. Merida, "A review of PEM fuel cell durability: degradation mechanisms and mitigation strategies", *J. Power Sources*, **184**, 104-119 (2008)

72. X. Yu and S. Ye, "Recent advances in activity and durability enhancement of Pt/C catalytic cathode in PEMFC Part Ⅱ: Degradation mechanism and durability enhancement of carbon

supported platinum catalyst", *J. Power Sources*, **172**, 145-154 (2007)

73. M. A. Rubio, A. Urquia, and S. Dormido, "Diagnosis of performance degradation phenomena in PEM fuel cells", *Int. J. Hydrogen Energy*, **35**, 2586-2590 (2008)
74. F. S. Saleh and E. B. Easton, "Diagnosing degradation within PEM fuel cell catalyst layers using electrochemical impedance spectroscopy", *J. Electrochem. Soc.*, **159**, B546-553 (2012)
75. Z. Wang, P. Zuo, Y. Chu, Y. Shao, and G. Yin, "Durability studies on performance degradation of Pt/C catalysts of proton exchange membrane fuel cell", *Int. J. Hydrogen Energy*, **34**, 4387-4394 (2009)
76. N. Cheng, S. Mu, M. Pan, and P. P. Edwards, "Improved lifetime of PEM fuel cell catalysts through polymer stabilization", *Electrochem. Commun.*, **11**, 1610-1614 (2009)
77. S. Kundu, M. Fowler, L. C. Simon, and R. Abouatallah, "Reversible and irreversible degradation in fuel cell during open circuit voltage durability testing", *J. Power Sources*, **182**, 254-258 (2008)
78. J. Healy, C. Hayden, T. Xie, K. Olson, R. Waldo, R. Brundage, H. Gasteiger, and J. Abbott, "Aspects of the chemical degradation of PFSA ionomers used in PEM fuel cells", *Fuel cells*, **5**, 302-308 (2005)
79. D. E. Curtin, R. D. Lousenberg, T. J. Henry, P. C. Tangeman, and M. E.

Tisack, “Advanced materials for improved PEMFC performance and life”, *J. Power Sources*, **131**, 41-48 (2004)

80. H. Tang, S. Peikang, S. P. Jiang, F. Wang, and M. Pan, “A degradation study of Nafion proton exchange membrane of PEM fuel cells”, *J. Power Sources*, **170**, 85-92 (2007)
81. R. M. Darling, and J. P. Meyers, “Kinetic model of platinum dissolution in PEMFCs”, *J. Electrochem. Soc*., **150**, A1523-A1527 (2003)
82. K. Yasuda, A. Taniguchi, T. Akita, T. Ioroi, and Z. Siroma, “Characteristics of a platinum black catalyst layer with regard to platinum dissolution phenomena in a membrane electrode assembly”, *J. Elctrochem. Soc.*, **153**, A1599-A1603 (2006)
83. A. Honji, T. Mori, K. Tamura, and M. Hishinuma, “Agglomeration of platinum particles supported on carbon in phosphoric acid”, *J. Electrochem. Soc*., **135**, 355-359 (1988)
84. K. Kinoshita, “Electrochemical oxygen technology”, John Wiley & Sons, New York, 1992.
85. K. Kinoshita, “Carbon. electrochemical and physicochemical properties”, John Wiley & Sons, New York, 1988.
86. H. R. Colon-Mercado and B. N. Popov, “Stability of platinum based

alloy cathode catalysts in PEM fuel cells", *J. Power Sources*, **155**, 253-263 (2006)

87. H. R. Colon-Mercado, H. Kim, and B. N. Popov, "Durability study of Pt_3Ni_1 catalysts as cathode in PEM fuel cells", *Electrochem. Commun*., **6**, 795-799 (2004)
88. S. J. Bae, S. J. Kim, J. I. Park, J. H. Lee, H. Cho, and J. Y. Park, "Lifetime prediction through accelerated degradation testing of membrane electrode assemblies in direct methanol fuel cells", *Int. J. Hydrogen Energy*, **35**, 9166-9176 (2010)
89. R. Lin, B. Li, Y. P. Hou, and J. M. Ma, "Investigation of dynamic driving cycle effect on performance degradation and micro-structure change of PEM fuel cell", *Int. J. Hydrogen Energy*, **34**, 2369-2376 (2009)
90. R. Makaharia, S. Kocha, P. Yu, A. Sweikart, W. Gu, F. Wagner, and H. A. Gasteiger, "Durability and reliability of low-temperature fuel cells systems", *ECS Trans*., **1**, 3-18 (2006)
91. X. Zhang, H. Wang, J. Key, V. Linkov, S. Ji, X. Wang, Z. Lei, and R. Wang, "Strain effect of core-shell Co@Pt/C nanoparticle catalyst with enhanced electrocatalytic activity for methanol oxidation", *J. Electrochem. Soc*., **159**, B270-276 (2012)

92. J. Luo, L. Wang, D. Mott, P. N. Njoki, Y. Lin, T. He, Z. Xu, B. N. Wanjana, I. I. Lim, and C. J. Zhong, ”Core/shell nanoparticles as electrocatalysts for fuel cell reactions”, *Adv. Mater*., **20**, 4342-4347 (2008)

93. D. Wang, H. L. Xin, Y. Yu, H. Wang, E. Rus, D. A. Muller, and H. D. Abruna, “Pt-decorated PdCo@Pd/C core-shell nanoparticles with enhanced stability and electrocatalytic activity for the oxygen reduction reaction”, *J. Am. Chem. Soc*., **132**, 17664-17666 (2010)

94. J. X. Wang, H. Inada, L. Wu, Y. Zhu, Y. M. Choi, P. Liu, W. Zhou, and R. R. Adzic, “Oxygen reduction on well-defined core-shell nanocatalysts: particle size, facet, and Pt shell thickness effects”, *J. Am. Chem. Soc*., **131**, 17298-17302 (2009)

95. A. Bayrakçeken, A. Smirnova, U. Kitkamthorn, M. Aindow, L. Türker, I. Eroglu, and C. Erkey, “Pt-based electrocatalysts for polymer electrolyte membrane fuel cells prepared by supercritical deposition technique”, *J. Power Sources*, **179**, 532-540 (2008)

96. A. Pozio, M. De Francesco, A. Cemmi, F. Cardellini, and L. Giorgi, “Comparison of high surface Pt/C catalysts by cyclic voltammetry”, *J. Power Sources*, **105**, 13-19 (2002)

97. M. Wilson, H. Garzon, K. Sickafus, and S. Gottesfeld, “Surface area

loss of supported platinum in polymer electrolyte fuel cells", *J. Electrochem. Soc.*, **140**, 2872-2877 (1993)

98. K. Sasaki, H. Naohara, Y. Cai, Y. M. Choi, P. Liu, M. B. Vukmirovic, J. X. Wang, and R. R. Adzic, "Core-protected platinum monolayer shell high stability electrocatalysts for fuel cell cathodes", *Angew. Chem. Int. Ed.*, **49**, 8602-8607 (2010)
99. L. Dubau, J. Durst, F. Marillard, L. Guetaz, M. Chtenet, J. Andre, and E. Rossinot, "Further insights into the durability of Pt_3Co/C electrocatalysts: formation of "hollow" Pt nanoparticles induced by the kirkendall effect", *Electrochim. Acta*, **56**, 10658-10667 (2011)
100. J. X. Wang, C. Ma, Y. M. Choi, D. Su, Y. Zhu, P. Liu, R. Si, M. B. Vukmirovic, Y. Zhang, and R. R. Adzic, "Kirkendall effect and lattice contraction in nanocatalysts: a new strategy to enhance sustainable activity", *J. Am. Chem. Soc.*, **133**, 13551-13557 (2011)

국문초록

고분자 전해질 연료전지는 차량용, 가정용 동력원으로 주목 받고 있다. 하지만 고분자 전해질 연료전지의 높은 제조 원가와 불완전한 안정성으로 인하여 상업화에 어려움을 겪고 있다. 따라서 촉매의 활성과 안정성을 증대시키면서 백금의 사용량을 줄일 수 있는 새로운 촉매에 대한 개발이 필요하다. 이러한 측면에서, 코어-쉘 촉매는 제조 원가를 낮추고 활성을 증대시킬 수 있는 장점을 지니고 있기 때문에 연료전지의 촉매로서 연구되고 있다. 그러나 코어-쉘 촉매를 단위전지와 같은 실제적인 시스템에 적용하거나 코어-쉘 촉매의 열화 현상에 대하여 평가한 연구는 아직 미흡하다.

본 연구에서는 실제적인 시스템에서 코어-쉘 촉매의 성능과 열화 특성에 대하여 평가하였다. 팔라듐-백금 코어-쉘 촉매와 상용 백금 촉매를 공기극에 적용하여 CCM 형태의 막전극 접합체를 제조하고, 이를 단위전지에 적용하였다. 단위전지에서 코어-쉘 촉매의 성능과 열화 현상을 평가하기 위하여 가속열화실험 전과 후에 전기화학적, 구조적 분석을 수행하였다. 코어-쉘 촉매와 백금 촉매의 열화 경향을 파악하기 위하여 로드 사이클링을 통한 가속열화실험을 수행하였다. 가속열화실험 전과 후의 구조적 분석을 위하여 HR-TEM,

XRD, XPS, FE-SEM 및 EDX 분석을 수행하였다. 그리고 전기화학적 특성을 평가하기 위하여 전류-전압 특성 및 CV 분석을 수행하였다.

Pd-Pt[0.5]/C와 Pd-Pt[0.7]/C 촉매를 이용한 단위전지의 초기 성능은 0.7 V에서 440 mA cm^{-2} 와 400 mA cm^{-2}로, 백금의 사용량을 감안한다면 상용 Pt/C 촉매를 사용한 성능(455 mA cm^{-2})과 비교할만한 수준이다. 가속열화실험 결과, Pt/C, Pd-Pt[0.5]/C 및 Pd-Pt[0.7]/C를 촉매로 사용한 MEA의 성능은 각각 39, 45 및 40% 감소하였다. 가속열화실험 초기 10시간동안 Pt/C를 사용한 MEA의 성능은 25% 감소한 반면, Pd-Pt[0.5]/C와 Pd-Pt[0.7]/C를 사용한 MEA는 각각 12와 1%의 성능 감소를 보였다. Pt/C를 사용한 경우 평가 초기에 성능이 급격하게 감소하며, 이후 완만하게 감소하였다. 반면에 Pd-Pt[0.5]/C와 Pd-Pt[0.7]/C를 사용한 MEA의 성능은 가속열화실험 동안 지속적으로 감소하였다. Pt를 사용한 MEA의 전기화학적 활성 면적은 크게 감소한 반면 팔라듐-백금 촉매를 사용한 MEA의 전기화학적 활성 면적은 거의 변화하지 않았다. Pt/C 촉매의 전기화학적 활성 면적 감소는 가속열화실험 중 나타난 단위전지 성능 감소와 연관 지을 수 있다. 가속열화평가 후, 팔라듐-백금 코어-쉘 촉매와 백금 촉매의 입자 크기는 증가하였다. 팔라듐-백금 촉매의 입자 크기 증가는 백금 촉매의 입자 크기 증가에 비하여 작게 나타났다. XPS, FE-SEM 및 EDX 분석에서 가속열화실험 후 팔라듐과 백금의 원소 구성비

는 변화하였으며, 멤브레인에서 팔라듐 띠를 확인할 수 있었다. 원소 구성비 분석을 통하여 가속열화실험 중 팔라듐-백금 코어-쉘 촉매의 팔라듐이 용출되었음을 판단할 수 있었다. 그리고 팔라듐의 용출 현상은 팔라듐-백금 촉매를 사용한 단위전지 성능의 감소와 연관 지을 수 있다. Pd-Pt[0.5]/C와 Pd-Pt[0.7]/C를 비교해보면 Pd-Pt[0.7]/C의 성능이 Pd-Pt[0.5]/C 보다 안정적이며, 이는 도포된 백금 양에 따른 영향으로 추정할 수 있다. 팔라듐-백금 코어-쉘 촉매의 안정성에 대한 결과는 가속열화실험 평가 전과 후의 XRD와 원소 구성비의 변화 결과와 일치하였다.

주요어: 고분자 전해질 연료전지, 성능감소, 가속열화실험, 막전극 접합체, 코어-쉘 촉매

학 번: 2006-30867